130/4-9 A+B Format
No Stock

GEAP-13620
AEC RESEARCH AND
DEVELOPMENT REPORT
JUNE 1970

MASTER

FAILED FUEL PERFORMANCE IN NATURALLY CONVECTING LIQUID METAL COOLANT

K. E. GREGOIRE
P. E. NOVAK
R. E. MURATA

U. S. ATOMIC ENERGY COMMISSION
CONTRACT AT(04-3)-189
PROJECT AGREEMENT 10

GENERAL ELECTRIC

DISTRIBUTION OF THIS DOCUMENT IS UNLIMITED

DISCLAIMER

This report was prepared as an account of work sponsored by an agency of the United States Government. Neither the United States Government nor any agency Thereof, nor any of their employees, makes any warranty, express or implied, or assumes any legal liability or responsibility for the accuracy, completeness, or usefulness of any information, apparatus, product, or process disclosed, or represents that its use would not infringe privately owned rights. Reference herein to any specific commercial product, process, or service by trade name, trademark, manufacturer, or otherwise does not necessarily constitute or imply its endorsement, recommendation, or favoring by the United States Government or any agency thereof. The views and opinions of authors expressed herein do not necessarily state or reflect those of the United States Government or any agency thereof.

DISCLAIMER

Portions of this document may be illegible in electronic image products. Images are produced from the best available original document.

LEGAL NOTICE

This report was prepared as an account of work sponsored by the United States Government. Neither the United States nor the United States Atomic Energy Commission, nor any of their employees, nor any of their contractors, subcontractors, or their employees, makes any warranty, express or implied, or assumes any legal liability or responsibility for the accuracy, completeness or usefulness of any information, apparatus, product or process disclosed, or represents that its use would not infringe privately owned rights.

GEAP 13620
AEC Research
and Development Report
June 1970

FAILED FUEL PERFORMANCE IN NATURALLY CONVECTING LIQUID METAL COOLANT

By

K. E. Gregoire
P. E. Novak
R. E. Murata

Approved: W. E. Baily
W. E. Baily, Project Engineer
Fast Ceramic Reactor Program

Approved: for E.L.Z.
E. L. Zebroski, Manager
Development Engineering

Prepared for the U.S. Atomic Energy
Commission under Contract AT(04-3)-189
Project Agreement No. 10

Printed in U.S.A. Available from the
Clearing House for Federal Scientific and Technical Information
National Bureau of Standards, U.S. Department of Commerce
Springfield, Virginia
Price $3.00 per copy

BREEDER REACTOR DEVELOPMENT OPERATION • GENERAL ELECTRIC COMPANY
SUNNYVALE, CALIFORNIA 94086

GENERAL ELECTRIC

6144-BRDO-56
225-EGO-1/71

DISTRIBUTION OF THIS DOCUMENT IS UNLIMITED

LEGAL NOTICE

This report was prepared as an account of Government sponsored work. Neither the United States, nor the Commission, nor any person acting on behalf of the Commission:

A. Makes any warranty or representation, expressed or implied, with respect to the accuracy, completeness, or usefulness of the information contained in this report, or that the use of any information, apparatus, method, or process disclosed in this report may not infringe privately owned rights; or

B. Assumes any liabilities with respect to the use of, or for damages resulting from the use of any information, apparatus, method, or process disclosed in this report.

As used in the above, "person acting on behalf of the Commission" includes any employee or contractor of the Commission, or employee of such contractor, to the extent that such employee or contractor of the Commission, or employee of such contractor prepares, disseminates, or provides access to, any information pursuant to his employment or contract with the Commission, or his employment with such contractor.

TABLE OF CONTENTS

APPENDIXES

LIST OF ILLUSTRATIONS

LIST OF TABLES

ABSTRACT

The results of an experiment are described in which two fuel specimens containing mixed oxide ($Pu_{0.25}U_{0.75})O_{2.0}$ were irradiated in NaK cooled natural circulation capsules in the GETR at power and temperature conditions in excess of those expected in current LMFBR designs. Both of the specimens failed at ≤18,000 MWd/Te. One of the specimens was immediately removed from the reactor after failure while the other was permitted to continue irradiation to 53,000 MWd/Te. Observation of both failed fuel pins showed significant transverse dimensional changes and fuel-cladding reaction.

1. SUMMARY

Two LMFBR type fuel pins containing ($Pu_{0.25}U_{0.75})O_2$ pellet fuel (B3B, B3C) were irradiated in the GETR pool in separate natural circulation capsules. The NaK-cooled pins were irradiated at heat ratings of 22 and 20 kW/ft with calculated peak cladding inside surface temperatures of 1350°F and 1450°F, respectively (current LMFBR designs specify ≤1250°F maximum cladding ID temperature). Both pins failed at ≤ 18,000 MWd/T burnup. One was removed without an appreciable increase in burnup while the other continued its irradiation at reduced power (18 kW/ft) and cladding inside surface temperature (1250°F) to an exposure of ~ 53,000 Mwd/T (peak) before removal.

Post-irradiation examination and analysis of the operating history of the experiments indicated the cause of failure in both specimens to be severe cladding degradation resulting from fuel cladding interactions at the high operating temperatures.

In one of the specimens (B3B), the complete depressurization of the fuel pin due to loss of gas from the pin after failure was observed to require about four hours. This indicates restricted gas flow between the gas plenum and the clad rupture zone some 14 inches below.

Diametral expansion occurred in both specimens, reaching a maximum of 34% in the ruptured zone of the initially hotter specimen that was operated for several months after failure (B3C). Diametral expansion of 20% was observed in the ruptured zone of the cooler specimen that was removed shortly after failure (B3B).

Fission gas release was found to be 64% in B3B and 63% in B3C. The results are similar to release rates in unfailed fuel.

NaK coolant system contamination from released fuel and fission products was significantly greater in the specimen that continued to operate with failed fuel compared to the specimen shut down soon after failure.

2. CONCLUSIONS AND OBSERVATIONS

1. Four hours were required for the fission gas pressure measured in the plenum of failed fuel pin B3B to drop from 76 psig to 25 psig (ambient). This long depressurization time was probably caused by closing of the fuel cladding gap during unfailed operation and suggests that the loss of pressure from failed LMFBR fuel may be correspondingly slow.
2. Subsurface and intergranular attack of austenitic stainless steel cladding in contact with ($Pu_{0.25}U_{0.75})O_2$ was less than 0.001 inch at 1150°F. Depth of corrosion increased with increasing temperatures.
3. Diametral increases of up to 34% occurred in 1/4 inch diameter pelleted $(0.75U - 0.25Pu)O_2$ mixed oxide fuel rods, ruptured during overpower operation (≥20 kW/ft) in slowly flowing NaK after 5,500 MWd/Te burnup.
4. Fission gas release in failed pins did not differ significantly from that in unfailed gas bonded pins with comparable heat ratings for burnups up to 50,000 MWd/Te.
5. Further experimentation under closely controlled conditions is required to enable the prediction of failed fuel element behavior and performance in reactor cores.

3. INTRODUCTION

Knowledge of the magnitude and rate of distortion of failed LMFBR fuel pins and the amount of fuel and fission products released from these failed elements during normal power operation is necessary to determine the overall availability and performance of an LMFBR power plant. This report describes the results of an experiment in which two mixed oxide fuel rods were unintentionally failed while operating at abnormally high temperatures. One fuel pin was allowed to run in flowing NaK for four months after failure, while the other pin was removed soon after failure.

4. EXPERIMENT DESCRIPTION

The experiment consisted of two mixed oxide fuel pins (designated B3B and B3C) with active fuel lengths of 23 and 20 inches respectively with each pin enclosed in a natural convection capsule with approximately 700 cc of circulating NaK coolant. Goal exposure was 100,000 MWd/Te for each specimen. Irradiation was conducted in the GETR pool at peak power levels of 22 and 20 kW/ft respectively. Fuel pin and capsule design details are given in Appendices A and B. The capsule design has also been discussed in detail previously.[1]

The two specimens, B3B and B3C, were designed and operated to have centerline temperatures at the fuel blanket interface of 950°C (1750°F) and 1925°C (3500°F) respectively. These temperatures were chosen to simulate peripheral and central pins in a typical 1000 MWe LMFBR.[2] Both fuel pins were fitted with continuous in-pile pressure sensors. The capsules were irradiated in V-RAFTs* capable of vertical and radial adjustment in the test reactor to permit accurate control of specimen power.[3]

Examination of the fuel specimens and capsules were conducted at the Radioactive Materials Laboratory at the General Electric Vallecitos Nuclear Center near Pleasanton, California.

5. IRRADIATION HISTORY

Both capsules operated routinely at rated power (22 and 20 kW/ft) during the first month of irradiation. During this time, critical capsule parameters such as temperatures and fission gas pressure in the fuel pin were continuously monitored and recorded. Figure 5-1 shows the fission gas pressure buildup in the fuel pin plenum of B3B in this period of time. Also shown in Figure 5-1 is the plot of the cladding temperature monitor thermocouple which was used to calculate fuel heat rating. The pressure sensor in B3C failed shortly after reactor insertion and did not function throughout the test.

At the beginning of the second month of irradiation, the erratic behavior of one of the thermocouples monitoring the peak cladding temperature in B3C forced operators to reduce the heat generation of the specimen for a few minutes. The power was subsequently brought back up to ~ 18kW/ft with a peak cladding i.d. temperature of ~ 1250°F. No further erratic thermocouple behavior was noted and this mode of operation was maintained throughout the remainder of the irradiation of B3C. It was not considered conclusive at the time, but the erratic thermocouple behavior probably signalled the failure of the B3C pin.

An estimated 10 to 25% overpower occurred in both fuel specimens during the reactor startup at the beginning of the third month of the scheduled irradiation. At that time, a decrease in the gas pressure within the B3B pin was observed (Figure 5-2). Several small temperature transients were detected by one of the thermocouples adjacent to the cladding in B3B at about the same time as the gas pressure began to decay. The capsule position was adjusted in small steps during a four-hour period to lower the fission power and avoid overheating the cladding. Twenty hours after the initial decrease in the fission gas pressure was observed, the VRAFT was adjusted to place the test specimen in a minimum power position (less than 5 kW/ft and 300°F cladding temperature) where it stayed for four weeks until removal from the test reactor.

During the fourth month of irradiation, a gradually rising temperature pattern in the B3C cold trap became evident, indicating an accumulation of fuel in that region due to failure of the fuel pin. The plot of the rising temperature pattern in the B3C cold trap is shown in Figure 5-3.

* Vertically and Radially Adjustable Facility Tube

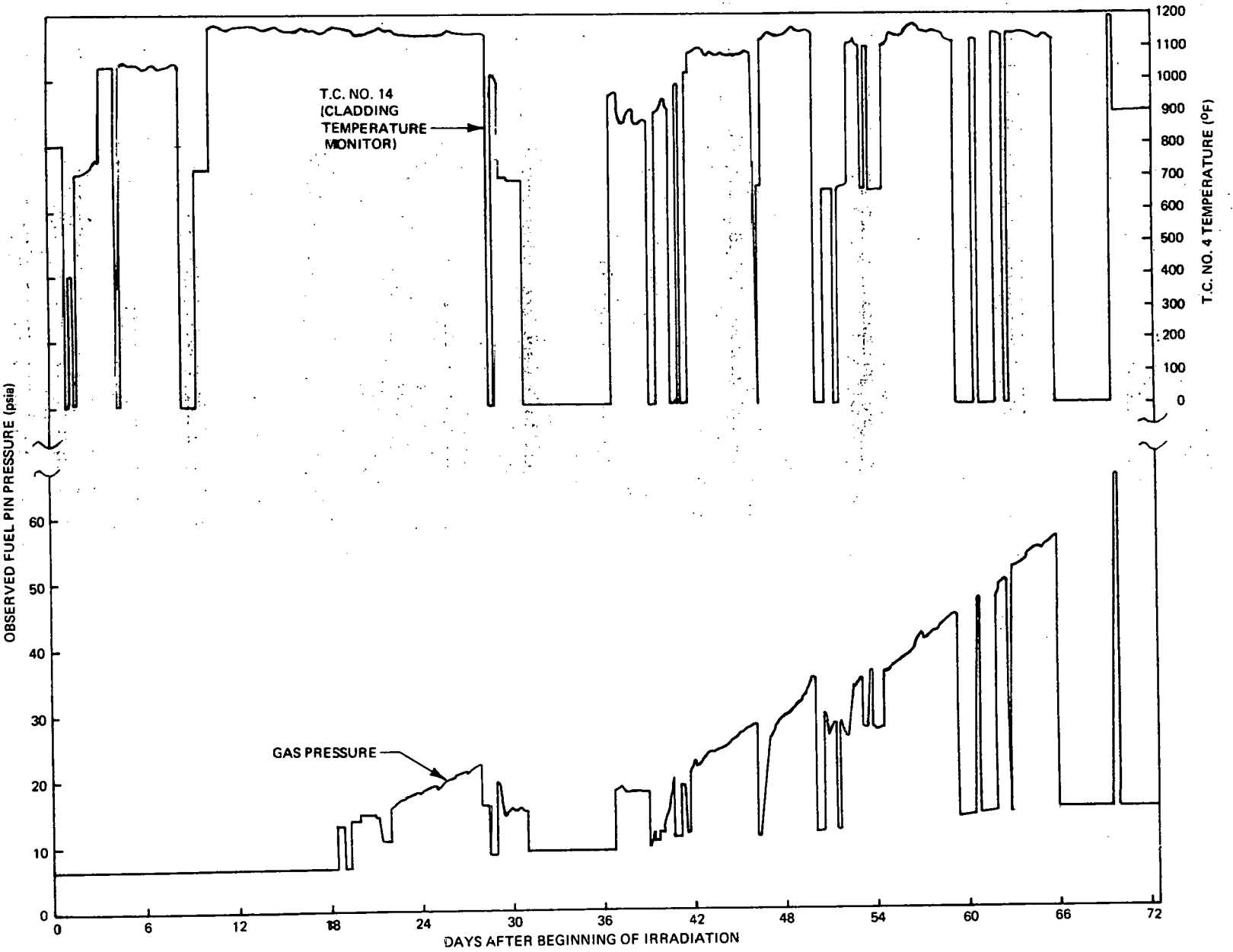

Figure 5-1. B3B Fuel Pin Pressure Buildup

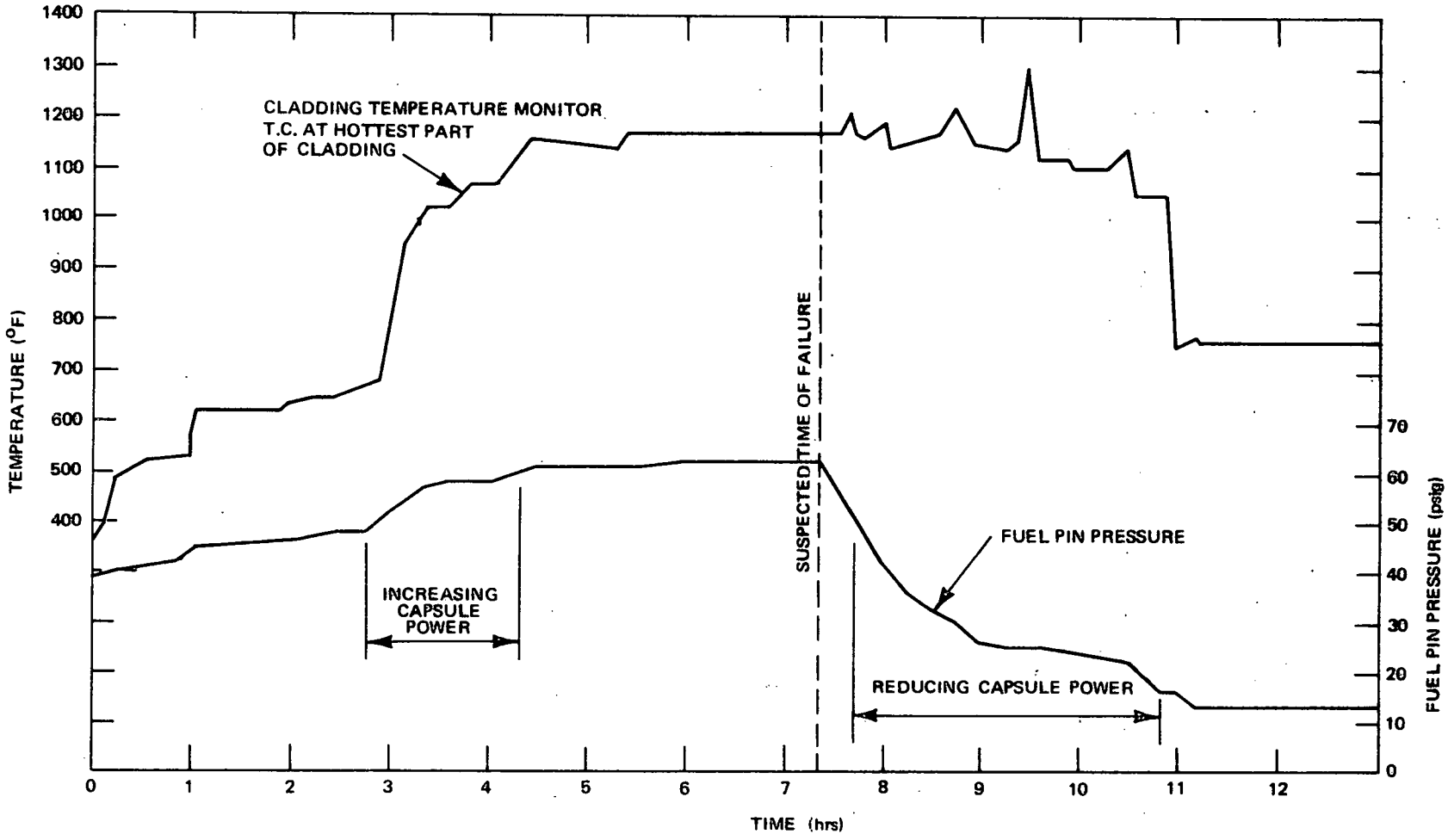

Figure 5-2. Critical Data for B3B Capsule at Time of Failure

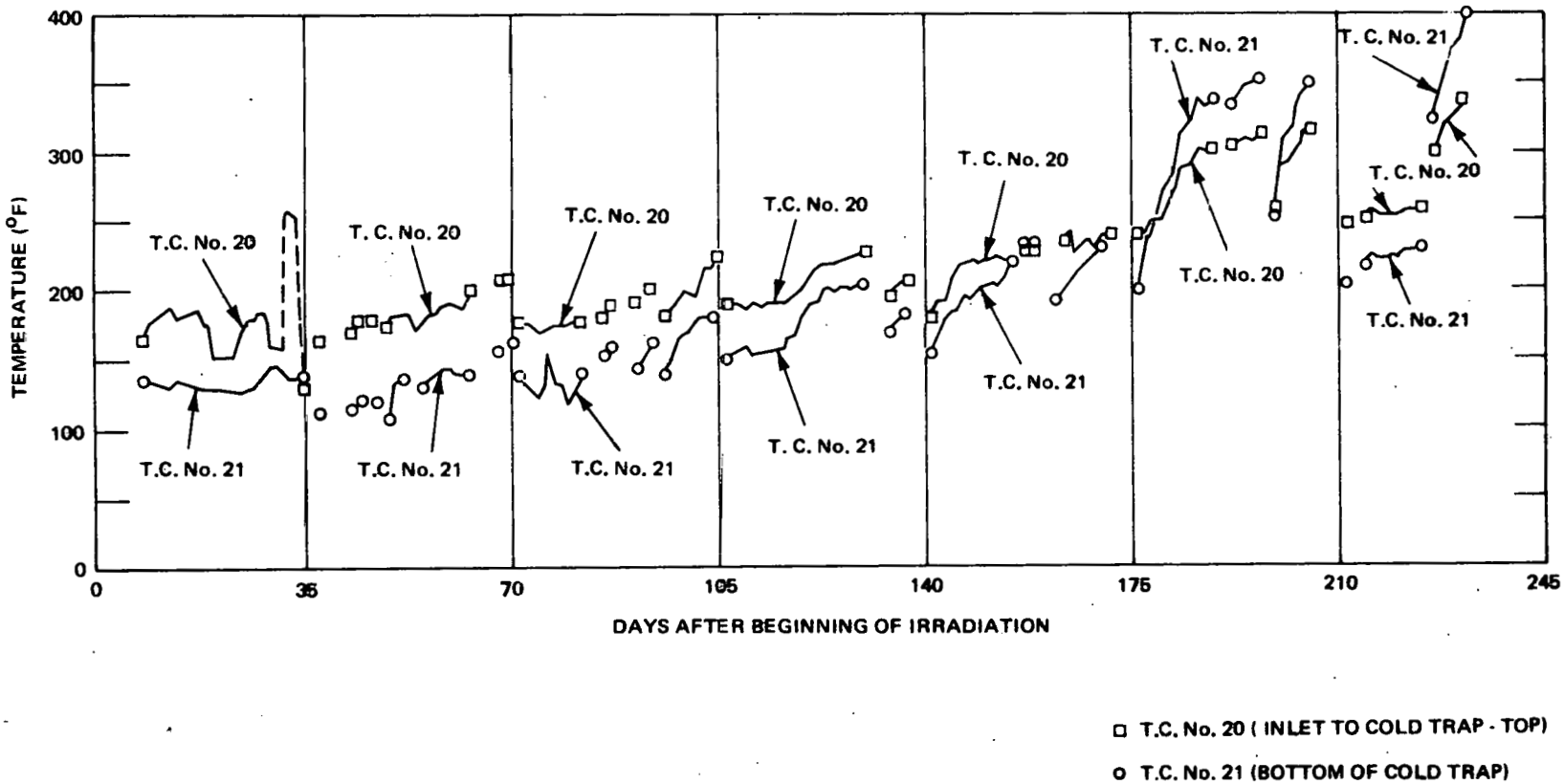

Figure 5-3. B3C Cold Trap Temperature History

B3C was subsequently removed from the reactor after seven months of exposure.

Capsules B3B and B3C experienced 22 and 39 power cycles during their respective irradiations.

6. POST-IRRADIATION EXAMINATION

The two capsules were examined at the General Electric Radioactive Materials Laboratory (RML) located near Pleasanton, California.

6.1 NEUTRON RADIOGRAPHY

The neutron radiograph of the B3C fuel pin, part of which is shown in Figure 6-1, clearly shows the areas in the pin from which fuel was lost. These correspond to the regions of greatest diametral deformation. The fuel central void can also be seen in Figure 6-1. Some fuel pellet interfaces were visible near the ends of the fuel column (not shown in Figure 6-1) indicating lower power operation. Neutron radiography was not available at the time of the B3B examination.

6.2 GAMMA SCANS

Gross gamma scans of the two capsules were made prior to destructive examination (Figure 6-2). The gamma scan of B3B indicated that some fuel had escaped from the pin and was deposited on a ledge in the capsule below the bottom end of the fuel pin. The scan of B3C showed a larger degree of axial fuel redistribution. Large activity peaks observed along the B3C fuel column were due to ruthenium, zirconium, and lanthanum and corresponded to metallic fission product ingots in the fuel itself. Large activity peaks seen at points below the bottom end of the fuel pin were due to fuel accumulated on the turning vanes and in the cold trap on the capsule.

6.3 PHYSICAL EXAMINATION

The appearance of the two fuel pins after removal from the capsules is shown in Figure 6-3. B3B exhibited at least seventeen small unconnected ruptures of the cladding in a zone which extended from 9-1/2 to 17-1/2 inches from the bottom end of the pin. B3C had one large continuous rupture which started at a point 11-1/2 inches above the bottom of the pin and continued upward for approximately 5 inches. Significant loss of fuel from B3C was confirmed by visual examination.

Post-irradiation diametral measurements were made on both specimens and are shown in Figure 6-4. The pre-irradiation diameters were 0.250 inch for both rods. The measurements in the failed regions indicate maximum cross-sectional dimensions at each elevation including the edges of the ruptured cladding.

6.4 FUEL PIN METALLOGRAPHY

Center Melting of Fuel

Figures 6-5 and 6-6 show the sectioning diagrams for both fuel specimens. Center melting was noted in both specimens. Massive grain growth characteristic of ceramics resolidified from the melt are readily visible in Figure 6-7. Heavy etching of the fuel by the NaK made it impossible to determine the exact extent of fuel melting because porosity changes in the fuel structure were obliterated.

Fuel-Sodium Reaction Product

The two specimens differed significantly in the appearance of the fuel at the fuel cladding interface. In B3B, there was an extensive fuel-sodium reaction phase in all regions of the pin except in the small area where the largest diametral expansion occurred. In contrast, there was virtually no reaction phase present in B3C except in the low power regions at the ends of the fuel.

Clad Ruptures

In B3B, the cracks in the clad, both incipient and complete, were longitudinal and frequently observed to occur in parallel; that is, more than one crack at a given axial point. Examples of these parallel cracks are shown in Figure 6-8. Clad necking was associated with all of the cracks examined metallographically.

Clad Corrosion

Severe attack of the inside surface of the cladding was observed in both specimens. This attack appeared to have a strong temperature dependence as shown in Figure 6-9. In this figure, views of cladding damage at various axial positions along the B3C pin are shown. The same general pattern of temperature dependent cladding attack was exhibited by B3B. Figure 6-10 shows a large metallic ingot which was observed at the fuel cladding interface in B3B. Etching the ingot with 10% oxalic acid is seen to have caused a large effect, indicating a different composition than the cladding.

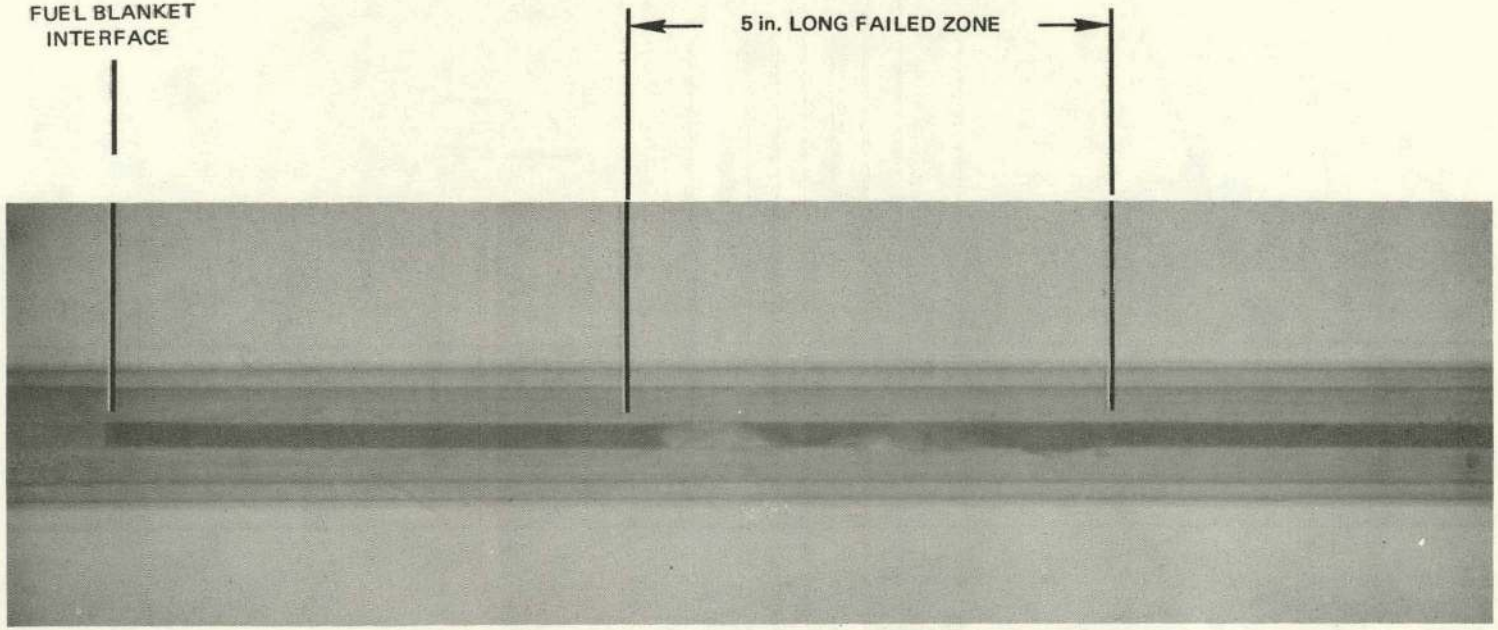

Figure 6-1. Neutron Radiograph Showing Failed Zone of B3C Fuel Pin

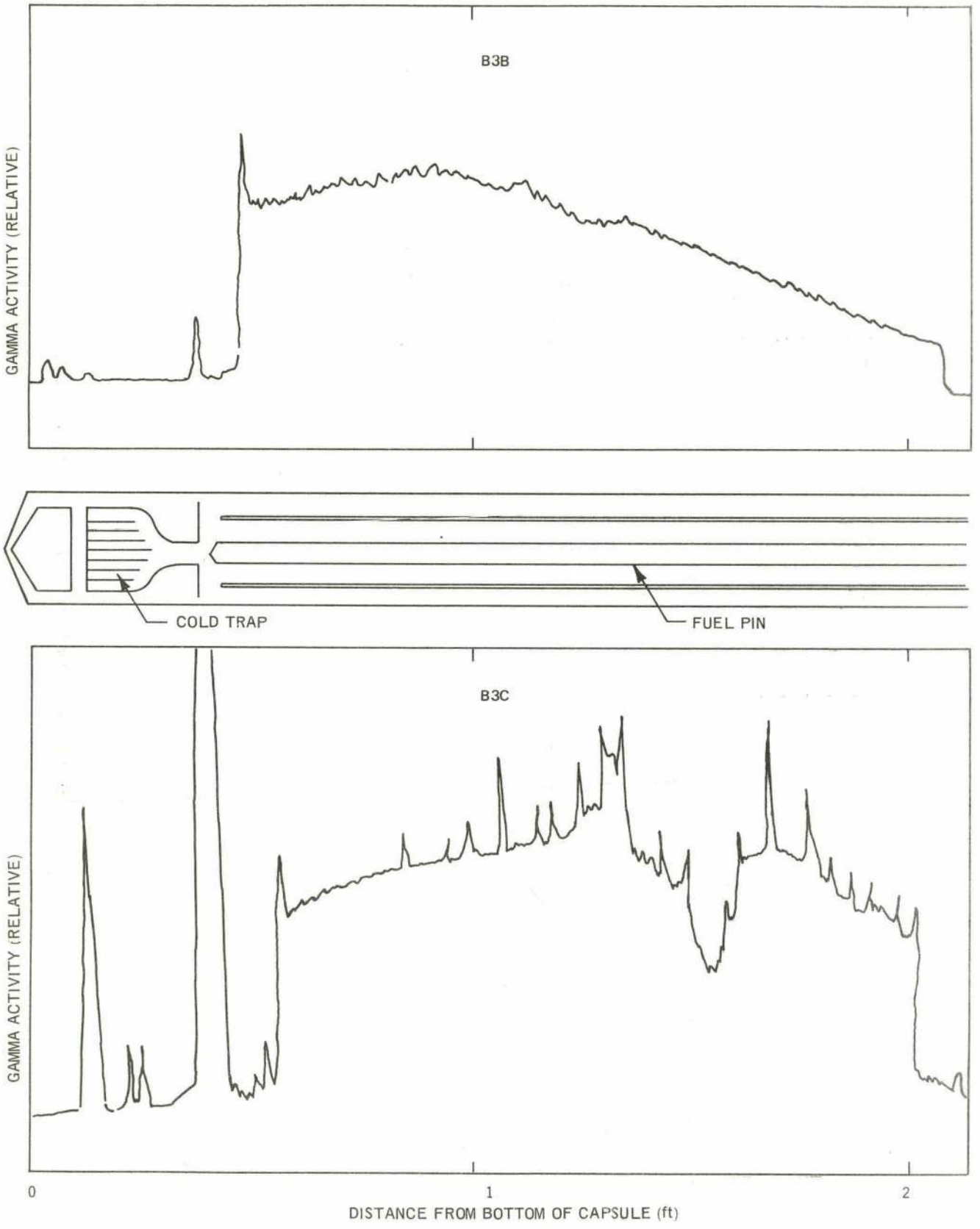

Figure 6-2. Gross Gamma Scans of B3B, B3C Capsules with Capsule Schematic

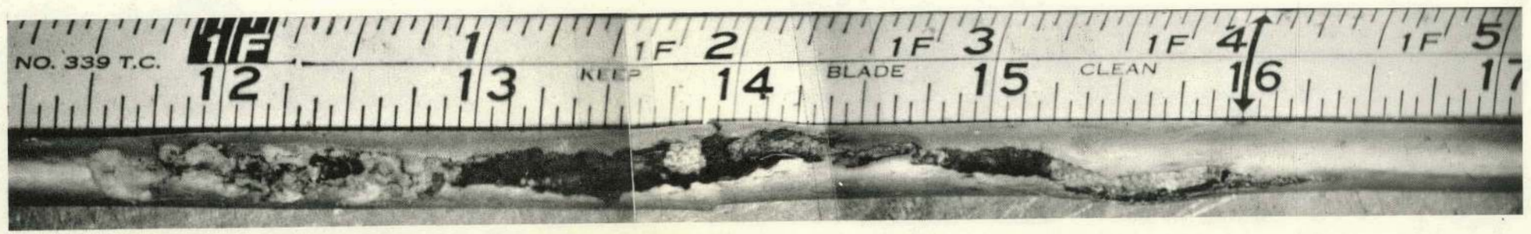

FUEL PIN B3C

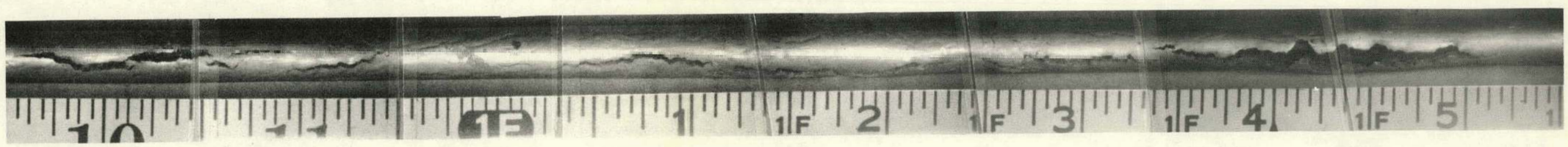

FUEL PIN B3B

Figure 6-3. Appearance of Failed Zones, B3B and B3C

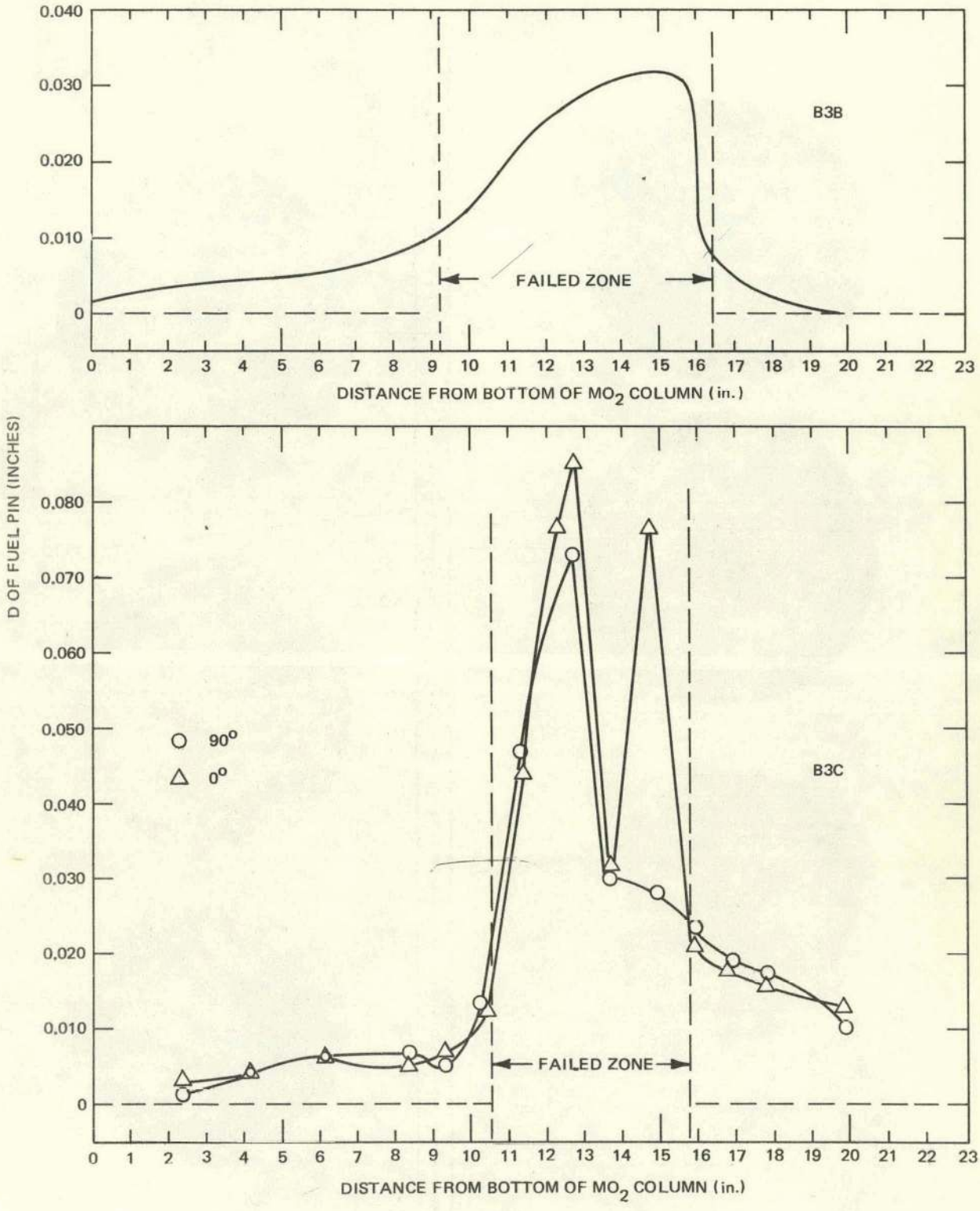

Figure 6-4. Post-Irradiation Fuel Rod Diameter Measurements

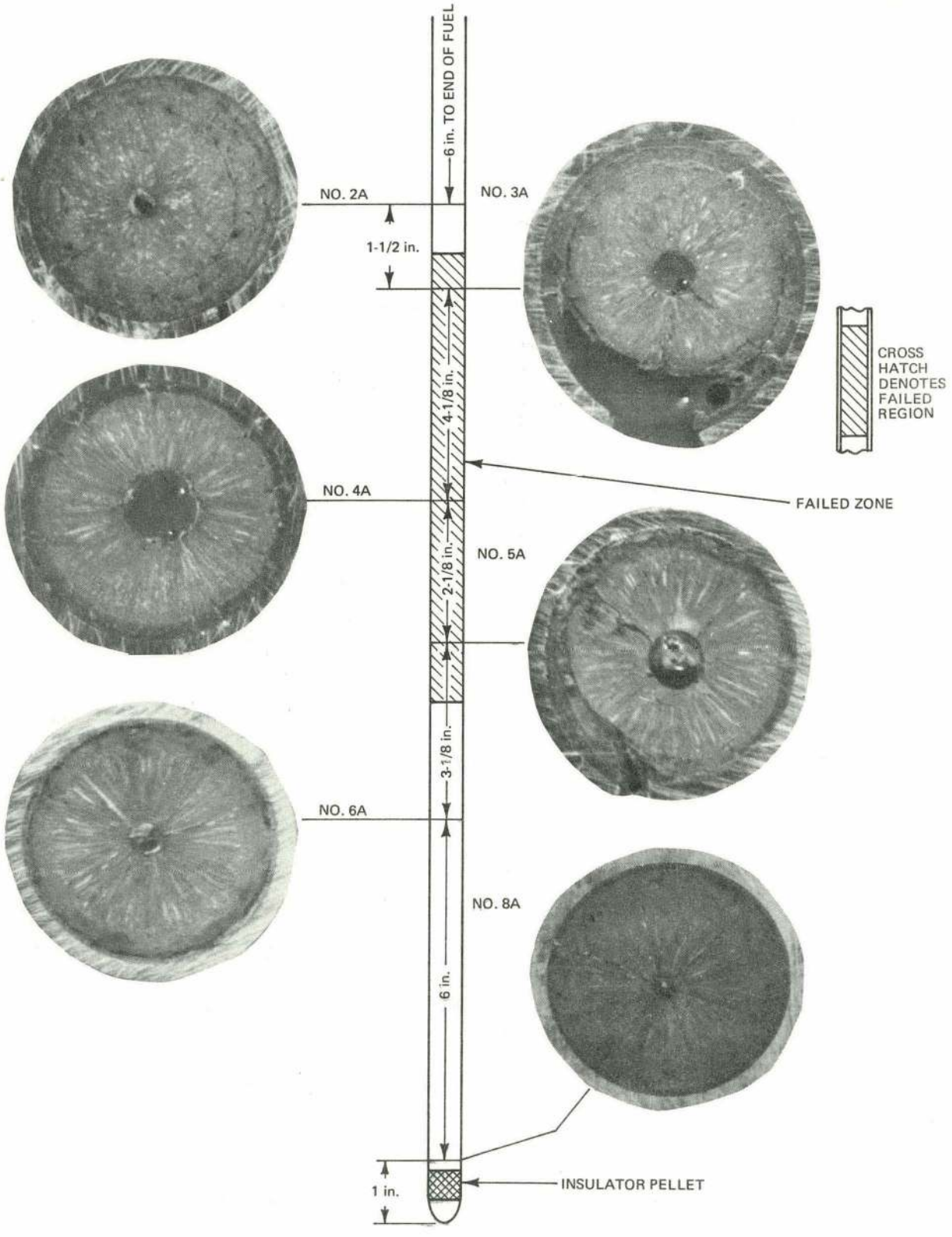

Figure 6-5. B3B Fuel Pin Sectioning Diagram

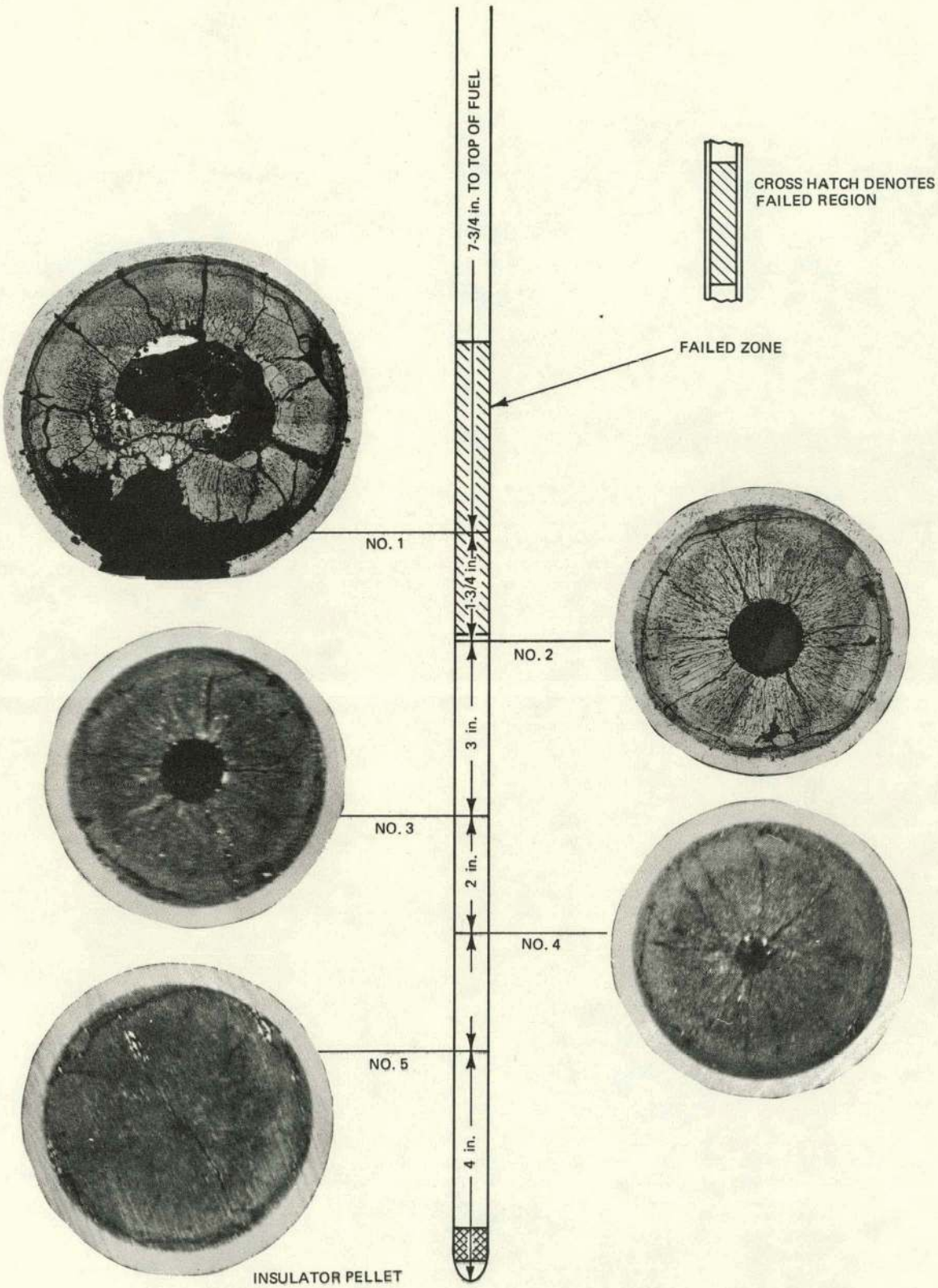

Figure 6-6. B3C Fuel Pin Sectioning Diagram

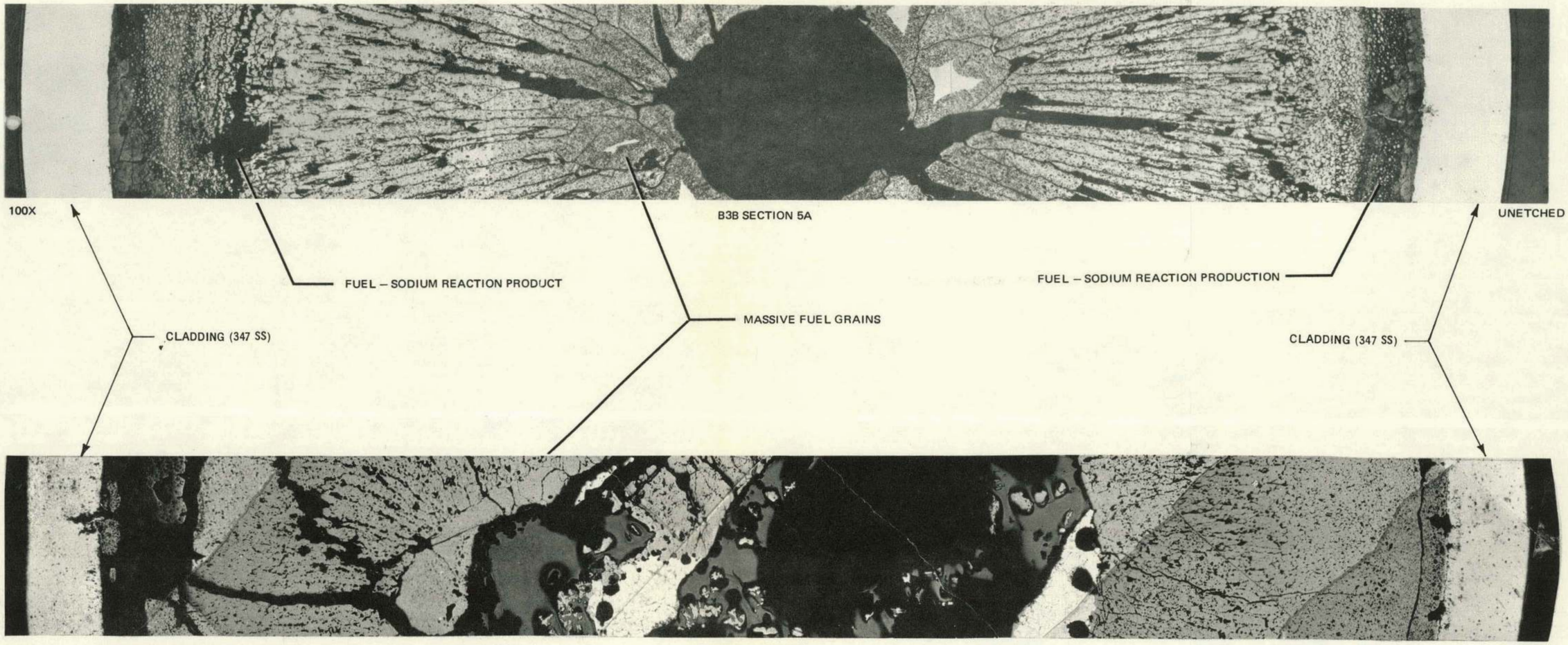

Figure 6-7. Typical Fuel Microstruture in Failed Zones of B3B, B3C Specimens

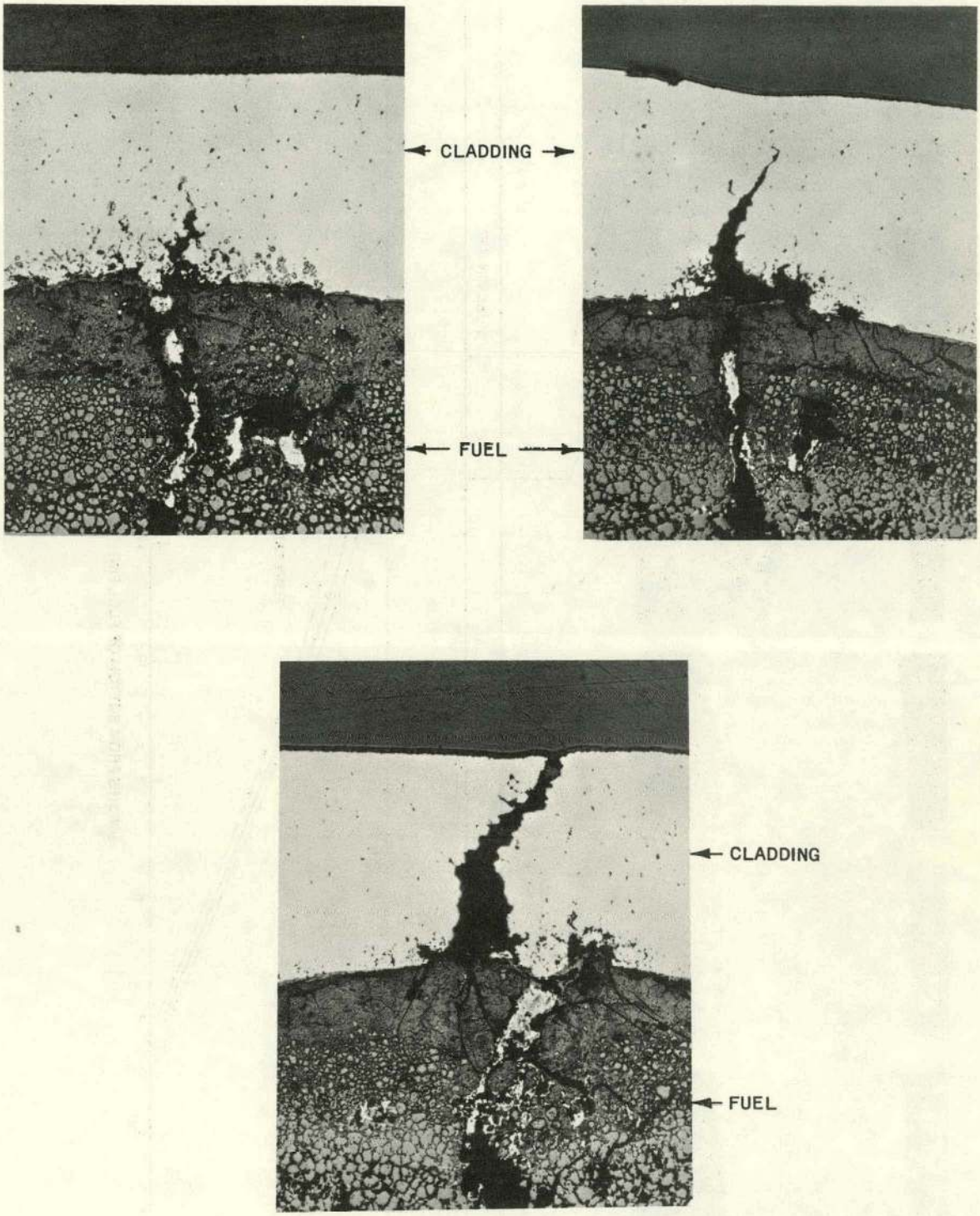

Figure 6-8. Three Parallel Cladding Ruptures in Section 4A of B3B Fuel Pin (100 X, Unetched)

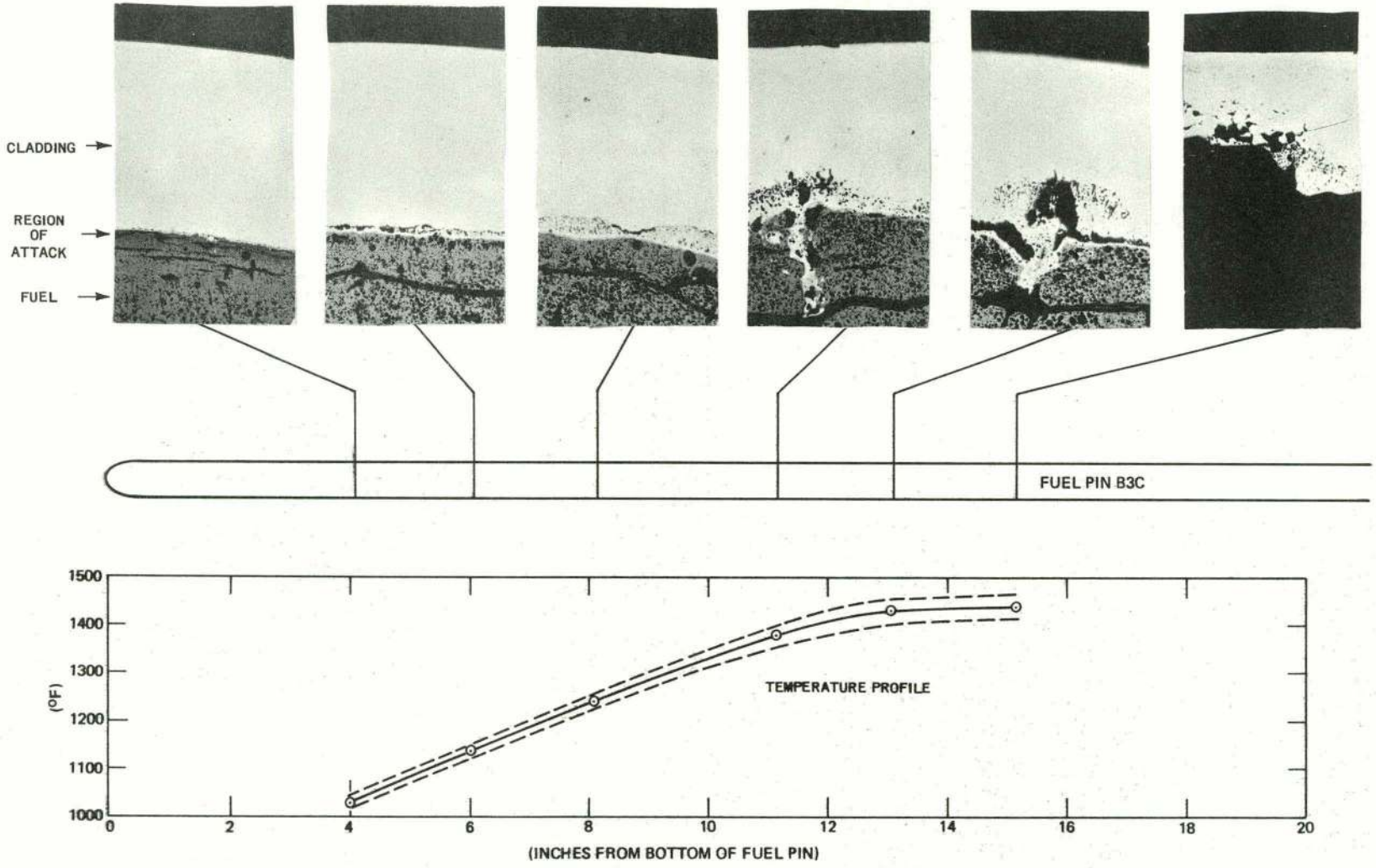

Figure 6-9. Varying Degrees of Attack on B3C Cladding

In both specimens, the metallic ingots and localized clad corrosion appeared to occur opposite radial cracks in the fuel as shown in Figures 6-6, 6-8 and 6-10.

Metallic Ingot

A large metallic ingot was found attached to an edge of the ruptured cladding of the B3C pin. Figure 6-11 shows the dendritic structure of the ingot after etching with 10% oxalic acid. The interface between the ingot and the adjoining cladding was examined closely for signs of a discontinuity. Also in Figure 6-11, it can be seen that the oxalic etch revealed a rather steep compositional gradient in this region where the ingot material was more sensitive to the etch than the cladding material.

The beta-gamma autoradiograph of the ingot indicated that it was of a composition other than that of the cladding. Figure 6-12 shows the higher beta-gamma activity of the ingot and also the activity of a smaller ingot located at the center of the fuel.

6.5 ELECTRON MICROPROBE EXAMINATION

The transverse section of B3C shown in Figure 6-12 was repolished and examined with an electron microprobe. Three areas were investigated:

1. The large metallic ingot attached to the cladding and the smaller metallic ingot in the fuel center were analyzed to determine the elements present. Full spectrometer scans were run at points "A", "B", and "C" in Figure 6-13. The fission product elements Mo, Te, Ru, Rh, and Pd were found to be present at all three locations in the same proportions. None of the major cladding constituents, Fe, Ni, or Cr, were detected at these three points.
2. The finger like extrusion extending from the inside surface of the cladding (point "D" in Figure 6-13) was also analyzed. Figure 6-14 notes a 250x photomicrograph of the extrusion. This micrograph shows that the extrusion is separated into two distinct regions. The first region is that area attached to the cladding, while the second region is separated from the first and elongated towards the center of the fuel pellet. Full spectrometer scans were obtained in both regions and taken of the major constituents. These indicate that the extrusion contained primarily cladding constituents. The first region of the extrusion contained the iron, nickel, and chromium in similar proportions to the cladding, itself. The second region, however, contained primarily iron with depletion of chromium and nickel. Figure 6-15 shows the distribution of iron, nickel, and chromium in the extrusion, and it is clearly seen that iron was present in high concentration in both regions. The chromium was evenly distributed in the first region and depleted in the second. The nickel concentration decreased as it approached the tip of the first region and was depleted in the second.
3. The cladding attack adjacent to the fuel matrix was also analyzed to determine which, if any, impurity elements were present. Full spectrometer scans were obtained at three points across the cladding thickness (pt. "D", Figure 6-13). These scans were run in order that the cladding could be standardized as to its elemental constituents, and the material at this point was found to contain major amounts of iron, nickel, and chromium, and minor amounts of manganese, molybdenum, niobium, silicon, and sulfur.

A fourth spectrometer scan was obtained (pt. "D", Figure 6-13) near the fuel for comparison with the clad scans. This region contained the above elements plus uranium, plutonium, ruthenium, and zirconium, and slightly more molybdenum than the unpitted clad region. Attempts were made to locate cesium along the cladding grain boundaries and in the heavily pitted region, but no cesium was found.

6.6 FISSION GAS ANALYSES

The mixture of fission gases and helium in B3C was collected and analyzed. The results of the analysis are summarized in Table 6-1. The trace amounts of nitrogen and argon are probably due to contamination from leaks during sampling. The helium was present as cover gas both within the pin and above the NaK at the beginning of irradiation.

6.7 COOLANT SYSTEM ANALYSES

Samples of the coolant from each capsule were obtained and analyzed by radio-chemical techniques. The results are summarized in Table 6-2. Samples CNA and BNA were obtained from the circulating NaK in B3C and B3B, respectively. Sample BNB was taken from the cold trap of B3B. The samples taken from B3B were analyzed for cesium only.

In addition, the B3B cold trap and two pieces of internal hardware from B3C were leached and the leach solutions analyzed for fission products and heavy metals. Table 6-3 shows the results of the leach sample analyses. Sample CLA was taken from the bottom end of the chimney and sample CLB was obtained from the upper end of the NaK reservoir. Locations of all NaK and hardware leach samples are shown in Figure 6-16.

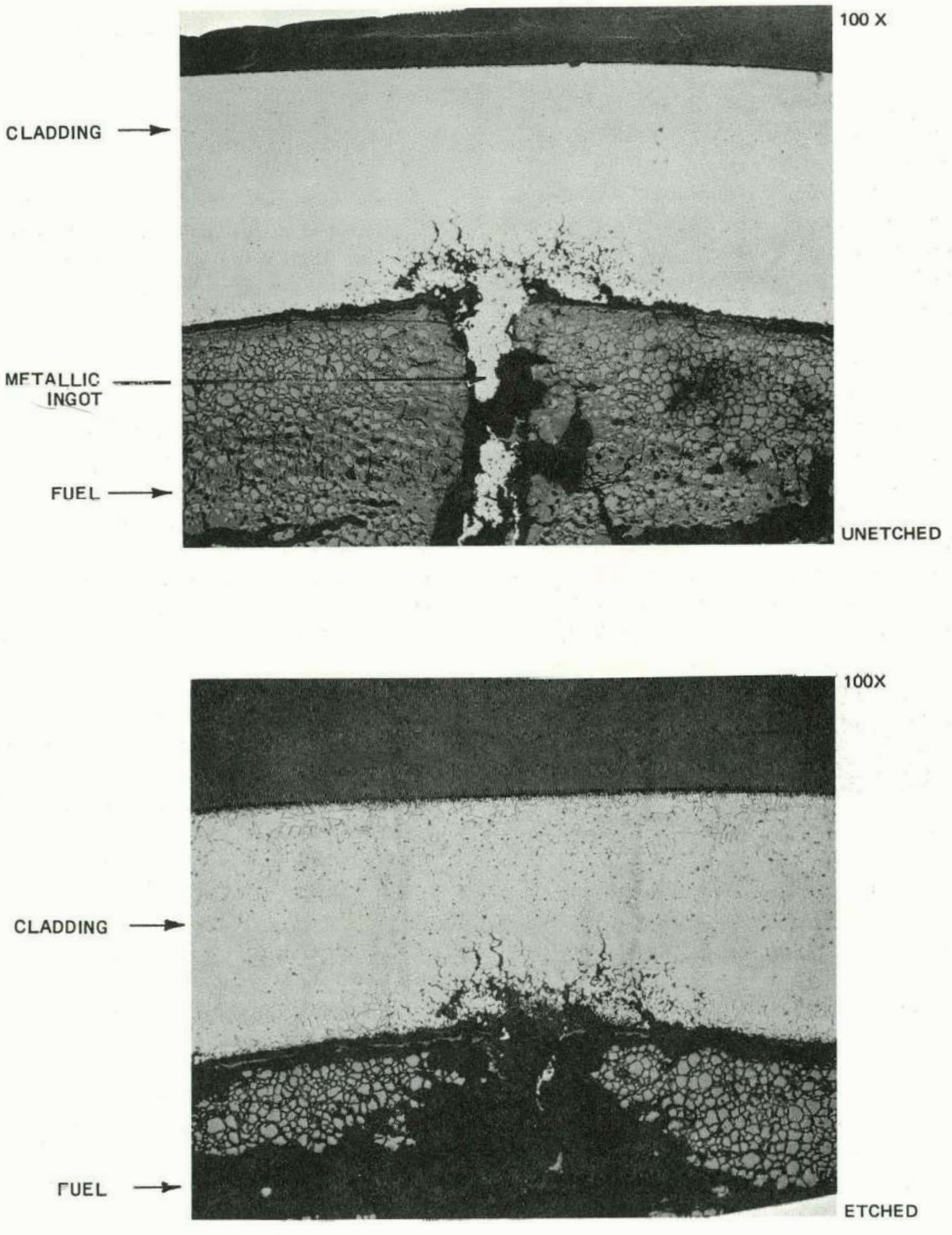

Figure 6-10. Example of Large Metallic Ingot in B3B

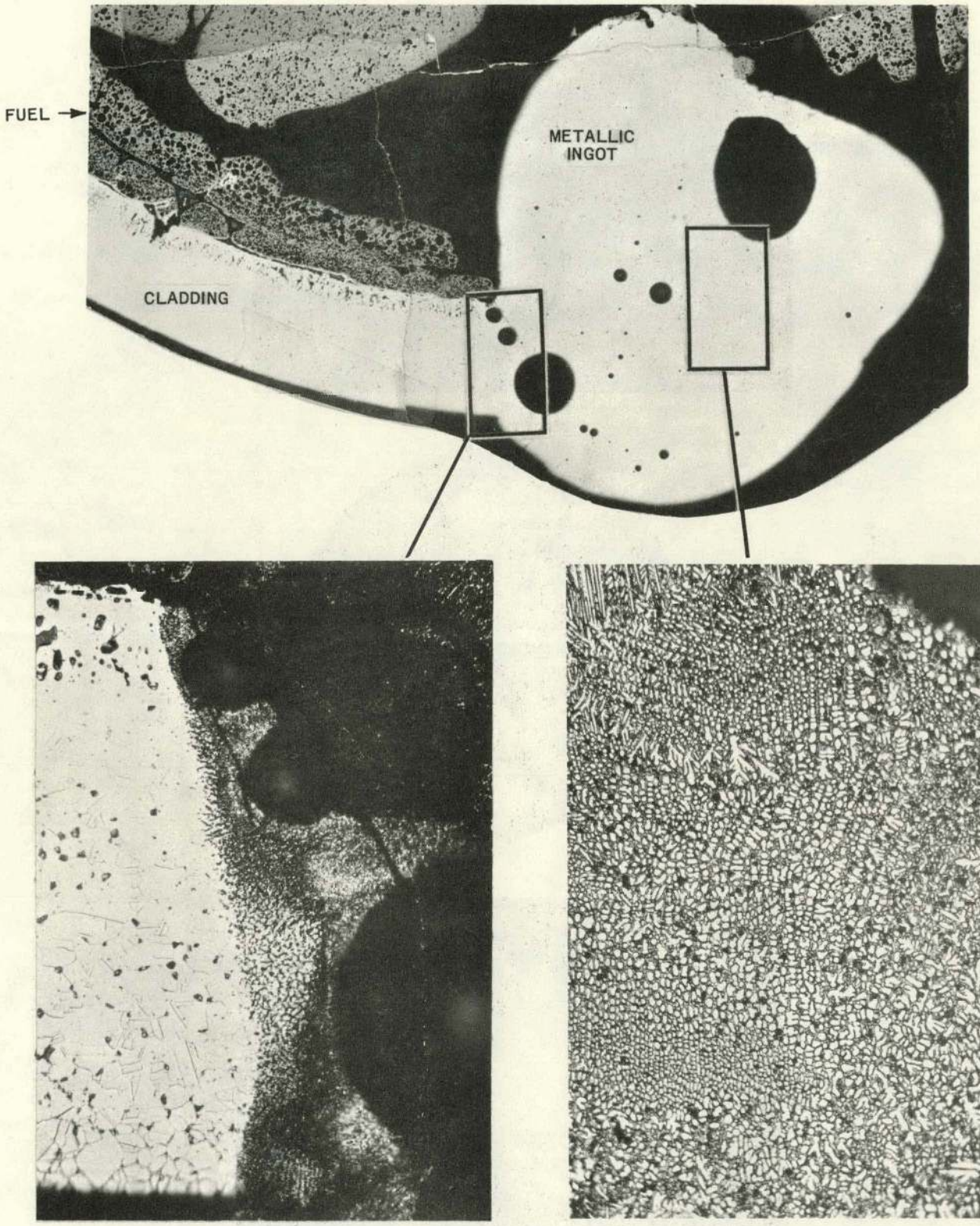

CONTRAST BETWEEN INGOT AND CLADDING AFTER ETCHING (B3C) WITH 10% OXALIC ACID

DENDRITIC STRUCTURE OF LARGE INGOT (B3C)

Figure 6-11. Appearance of Metallic Ingot after Etching

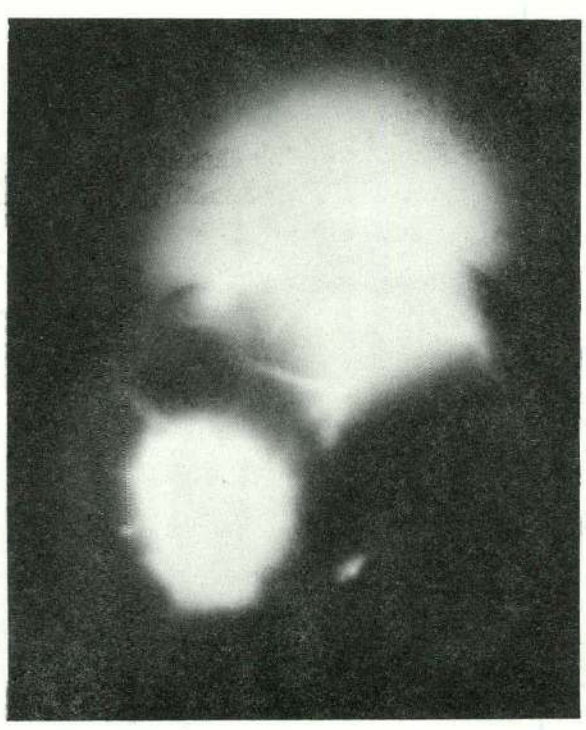

10 sec

MICROPHOTOGRAPH

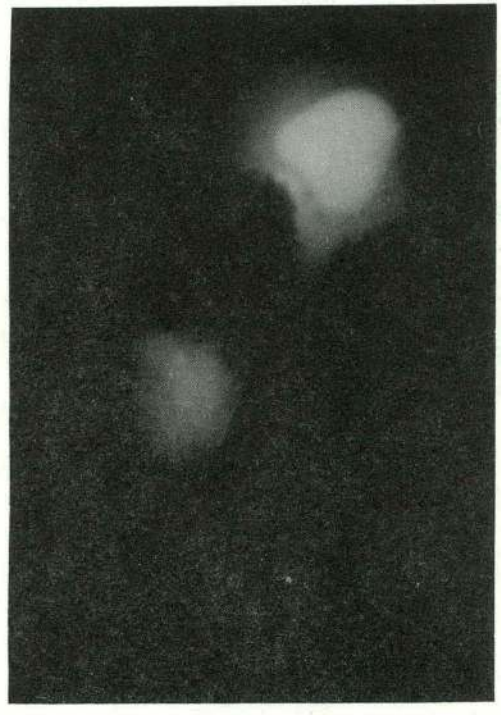

5 sec

Figure 6-12. Activity of Metallic Ingots at 5 and 10 Second Exposure (B3C)

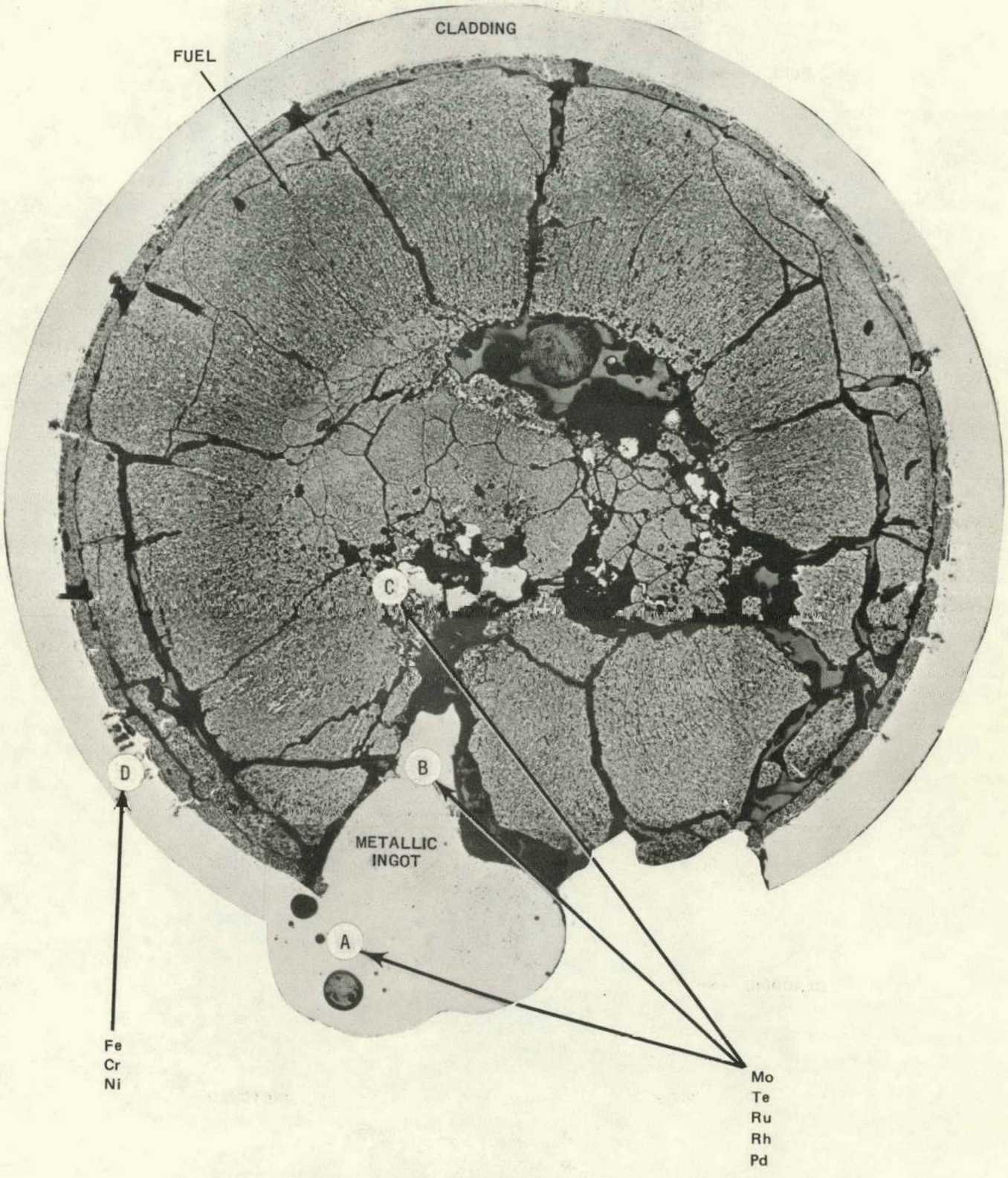

Figure 6-13. Microprobe Fuel Sample of B3C

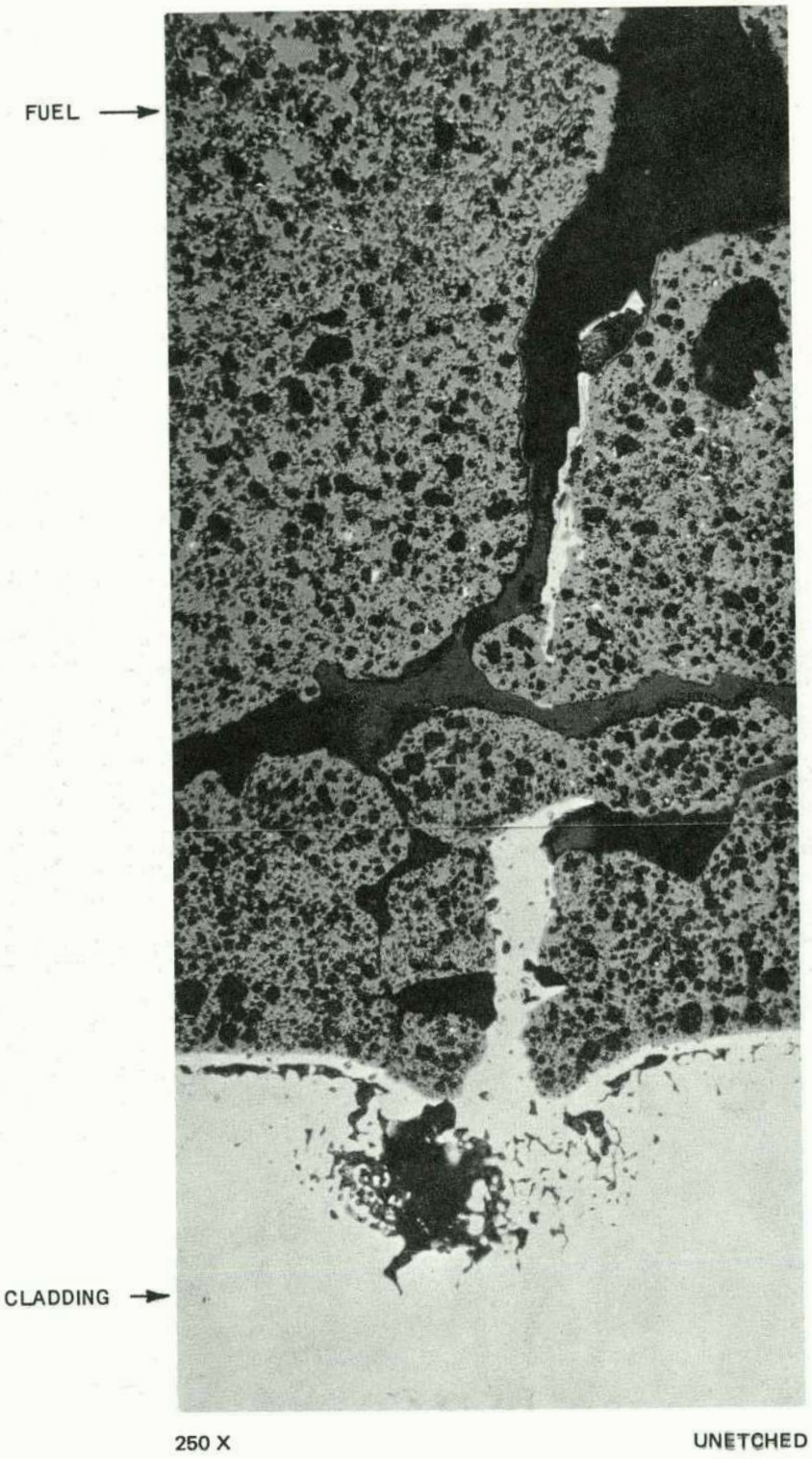

Figure 6-14. "Finger-Like" Extrusion Extending from the Inside Surface of Cladding (B3C)

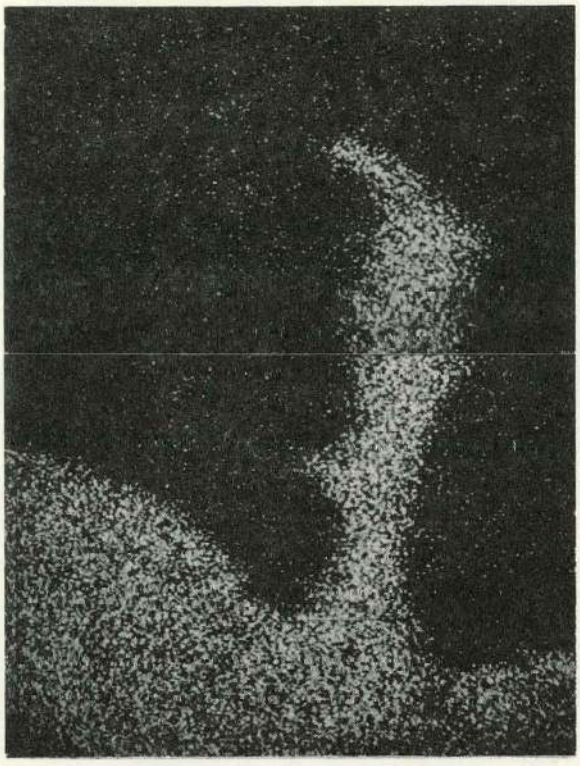

CHROMIUM DISTRIBUTION

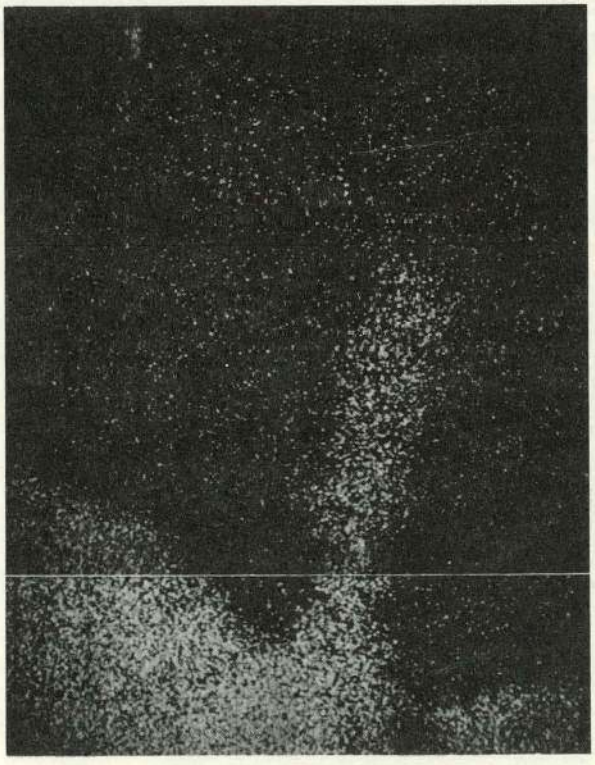

NICKEL DISTRIBUTION

IRON DISTRIBUTION

Figure 6-15. X-Ray Pulse Images of Cr, Ni, and Fe Distributions in B3C

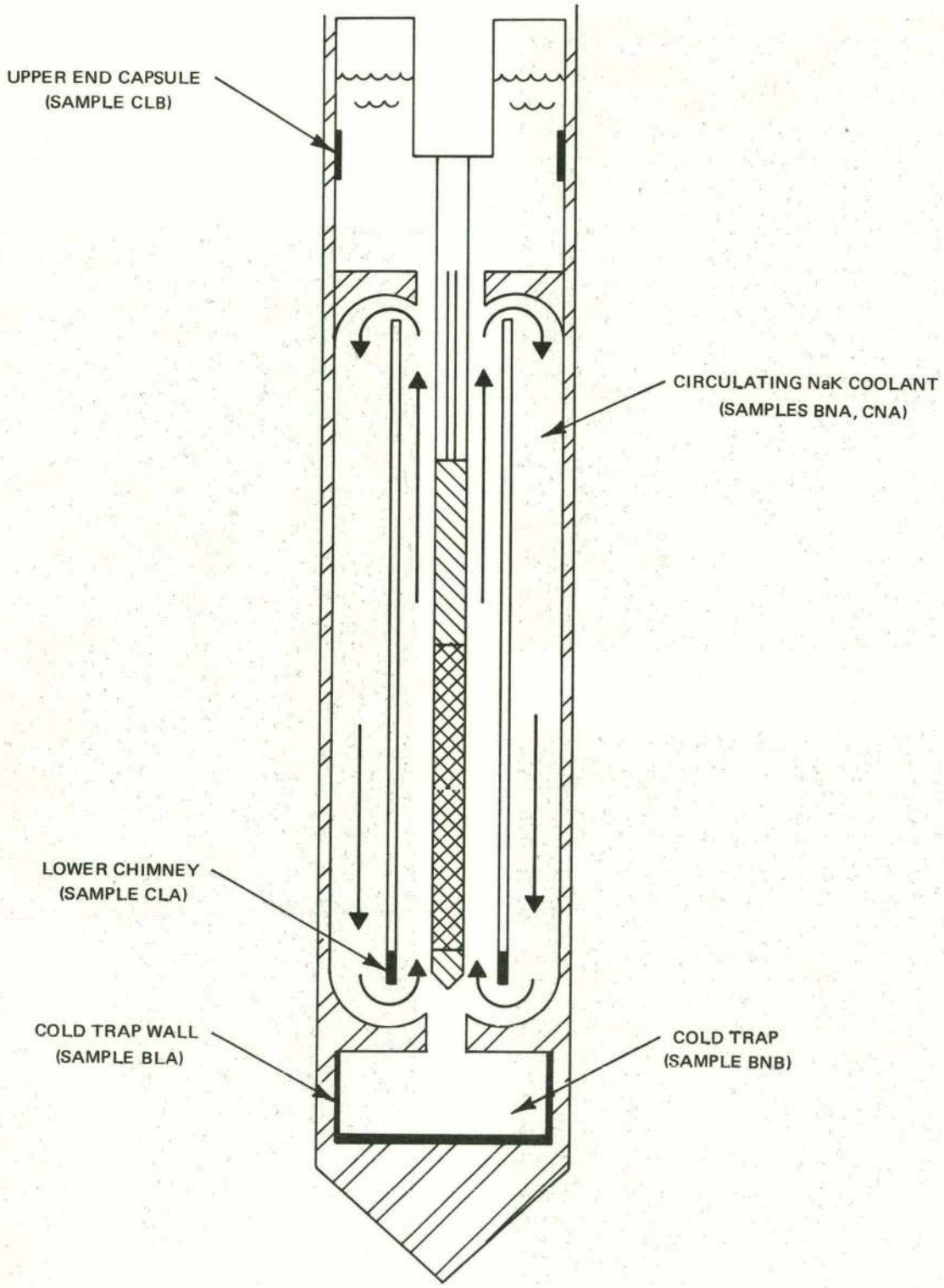

Figure 6-16. NaK and Hardware Leach Sample Locations (B3B, B3C)

Table 6-1
B3C FISSION GAS ANALYSIS RESULTS

Species	Percent of Total	Volume (cc)
Helium	56.2 ± 0.1	134.2
Xenon	34.6 ± 2.1	82.7
Krypton	3.0 ± 0.1	7.2
Argon	2.2 ± 0.1	5.3
Nitrogen	0.3 ± 0.1	0.7
Hydrogen	Not Detected	
Carbon Monoxide	Not Detected	
Methane	Not Detected	

Total Volume of Gas Sample = 239 cc (STP)

Table 6-2
B3B, B3C COOLANT ANALYSIS RESULTS

Atoms per Gm of Nak

Isotope / Source of Sample	B3B Sample BNA (Bulk Na)	B3B Sample BNB (Cold Trap Na)	B3C Sample CNA (Bulk Na)
Cs^{134}	7.7×10^{10}	8.6×10^{10}	2.4×10^{15}
Cs^{137}	4.4×10^{13}	4.6×10^{13}	2.1×10^{17}
Ce^{144}	Not Obtained		7.7×10^{10}
Ru^{106}	Not Obtained		4.2×10^{11}
Ru^{103}	Not Obtained		9.0×10^{13}
Sb^{125}	Not Obtained		1.3×10^{11}
Zr^{95}	Not Obtained		3.2×10^{12}
Y^{91}	Not Obtained		$< 8.9 \times 10^{14}$
Na^{22}	Not Obtained		1.2×10^{11}
Fe^{59}	Not Obtained		3.7×10^{13}
Co^{60}	Not Obtained		2.0×10^{11}
Pu^{239} *	Not Obtained		0.54×10^{-3}
Uranium*	Not Obtained		1.3

* μgm/gm Nak

Table 6-3
B3B, B3C LEACH SAMPLE ANALYSES RESULTS

Atoms per Square Inch of Sample Area

Isotope	B3B Sample BLA (100°F)	B3C Sample CLA (100°F)	B3C Sample CLB (200°F)
Cs^{134}	0.03×10^{10}	0.43×10^{12}	1.23×10^{13}
Cr^{137}	1.4×10^{10}	1.19×10^{13}	1.42×10^{15}
Ce^{144}	0.10×10^{10}	1.35×10^{11}	0.96×10^{15}
Ru^{106}	N.O.*	0.32×10^{12}	2.9×10^{14}
Ru^{103}	N.O.*	2.0×10^{13}	6.1×10^{15}
Sb^{125}	N.O.*	1.0×10^{14}	1.5×10^{14}
Zr^{95}	0.17×10^{10}	1.2×10^{12}	3.6×10^{14}
Y^{91}	N.O.	$< 7.1 \times 10^{13}$	$< 9.7 \times 10^{13}$
Na^{22}	N.O.	1.1×10^{10}	3.7×10^{11}
Fe^{59}	N.O.	2.8×10^{12}	1.2×10^{14}
Co^{60}	N.O.	1.8×10^{11}	1.1×10^{13}
Pu^{239}*	N.O.	0.053	12

* $\mu gm/in.^2$

*Not Obtained

7. DISCUSSION OF RESULTS

7.1 FISSION GAS PRESSURE DROP-OFF FROM FAILED PINS

The fuel pin pressure data shown in Figure 5-2 are unique in that this is the first time information concerning the rate of release of fission gas from a failed LMFBR-type fuel rod has been obtained. The volume of gas in the B3B pin at the time of rupture is calculated to have been ~ 33 cc (STP). The equilibrium volume of gas in the pin after failure is calculated to have been ~ 19 cc (STP). Thus, the indicated loss of gas during the 4-hour period of fuel pin pressure loss is ~ 14 cc (STP). The maximum gas release rate appears to have occurred during a 45-minute period immediately following the cladding rupture, and is estimated to have been at a rate of ~ 0.22 cc/min., or 3.8×10^{-3} cc/sec.

The apparent cause for the low gas flow rate is restriction of the passage between the plenum and the point of the cladding rupture. On this basis the "as fabricated" fuel cladding gap of 0.0028 inch must have been effectively closed by the swelling of the fuel to an equivalent gap of 1.4×10^{-7} inch (assuming laminar flow, uniform swelling of the six inch fuel column between the rupture and the plenum, and no flow interference from the nine inch blanket). The presence of liquid metal in the pin may also have inhibited the flow of gas since the surface tension of NaK is large and would be significant in small orifices. After penetration of the NaK, the fuel-NaK reaction phase would also tend to fill the available space in the fuel cladding gap, further restricting gas flow.

7.2 CLADDING CORROSION

The observed corrosion on the i.d. surfaces of the cladding in the B3B and B3C fuel pins is greater than that observed in out-of-pile tests[4] at comparable times and temperatures.

The depth of cladding attack observed in B3C is shown in Figure 7-1 plotted as a function of the maximum cladding temperature. Attack is evident at all points on the inside cladding surface of both specimens which operated in excess of 1100°F.

The location of most of the metallic "fingers" adjacent to radial cracks in the fuel in both specimens (Figure 6-6) suggests that these cracks do not completely disappear during operation. It appears that the outer-most ends of the cracks, which lie outside the sintering temperature isotherm, remain open at all times. Such perpetually open cracks may create avenues for fission product migration to the inside surface of the cladding of gas bonded fuel pins. These areas appear to be sites for accelerated cladding attack.

The cladding attack evident in B3B and B3C is not an isolated case but has been observed in many other failed and unfailed mixed oxide specimens. Zebroski, et al., were the first to observe the phenomenon during the examination of E2B[5], which was irradiated to 70,000 MWd/Te in the GETR with a peak power generation rate of ~ 18 kW/ft.

E5B-1 and -2, two mixed-oxide specimens successfully irradiated to over 100,000 MWd/t average burnup in thermal flux, had cladding temperature comparable to those of B3B and B3C.[6] These specimens also displayed cladding attack to depths of ~0.005 inch at the fuel cladding interface with large fingers of metallic material extending into the fuel from the cladding.

Another unfailed mixed oxide specimen, F2T, was irradiated to 74,000 MWd/T in EBR-II with peak cladding temperatures to about 300°F lower than those of B3B[7]. Metallic stringers were also found in this specimen adjacent to the cladding. However, the heavy cladding attack observed in B3B, and B3C was not observed. Another unfailed, vented mixed oxide specimen, B4D, was irradiated with peak fuel cladding interface temperatures of 1150 to 1175°F to ~ 45,000 MWd/T peak burnup in the GETR with results similar to those of F2T.[8]

Table 7-1 summarizes the mixed oxide specimens irradiated under this program* which have exhibited metallic fingers at the fuel cladding interface.

Details concerning E5B and F2T are given in Reference 9.

7.3 FUEL PIN DIMENSIONAL CHANGES

Kinetics

The large ingot of metallic fission product alloy discussed in Sections 6.3 and 6.4 was similar in appearance and composition to those seen many times in the center of mixed oxide fuel pins that operated under conditions of center melting. On this basis it is reasonable to assume that, prior to failure, this ingot was in the center of the B3C fuel.

Since the ingot was found fused to the cladding, its temperature necessarily exceeded the melting point of the clad (2700 to 2750°F) at the instant of contact between them. Also, since the ingot was probably surrounded by NaK at the moment of contact with the cladding, it was losing temperature quite rapidly. This means that the ingot must have migrated to its point of fusion with the cladding in a short period of time. However, since the fission

* Fast Ceramic Reactor Development Program

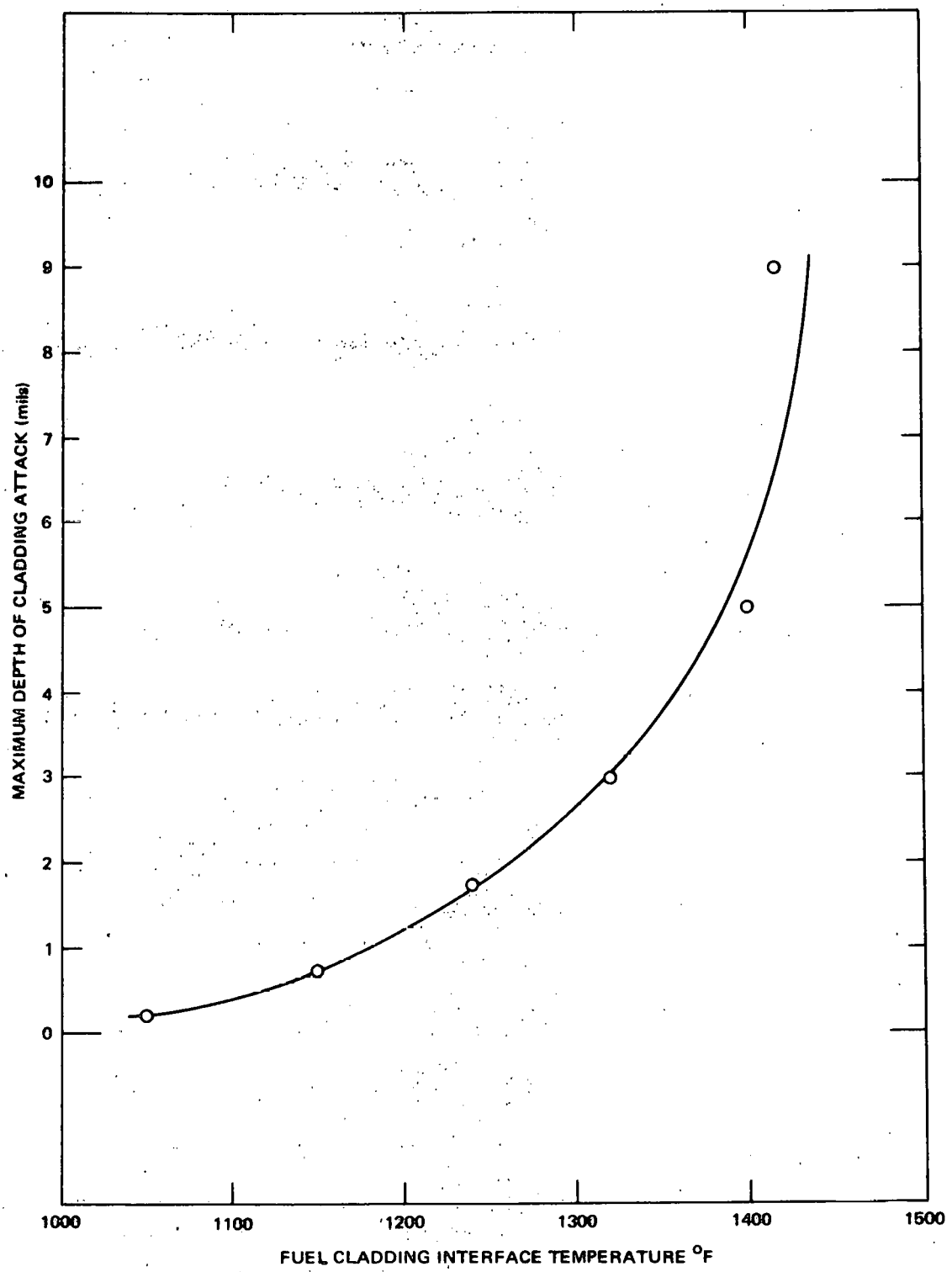

Figure 7-1. B3C Cladding Attack versus Fuel-Cladding Interface Temperature

Table 7-1
HELIUM-BONDED MIXED-OXIDE FUEL SPECIMENS
EXHIBITING METALLIC INCLUSIONS AT FUEL-CLAD INTERFACE

Specimen Designation	Failed	Reactor	Maximum Fuel-Clad Interface Temp.	Burnup
B3B	Yes	GETR	1350°F	18,000 MWd/Te
B3C	Yes	GETR	1450°F	53,000 MWd/Te
E2B-1	Yes	GETR	1150°F	70,000 MWd/Te
E5B-1	No	GETR	1400°F	100,000 MWd/Te
E5B-2	No	GETR	1400°F	100,000 MWd/Te
B4D	No	GETR	1200°F	46,000 MWd/Te
F2T	No	EBR-II	1100°F	74,000 MWd/Te

product ingot is not fused to both edges of the cladding, the two cladding edges must have been separated by a distance greater than the diameter of the ingot (0.085 inch) at the moment of fusion.

Separation of the cladding edges by 0.085 inch is equivalent to an 11% increase in the circumference of the fuel rod.

Magnitude

Pins B3B and B3C operated at atypically high cladding and fuel surface temperatures. However, the large transverse dimensional changes which occurred in these specimens can not be explained satisfactorily in the light of present day information. Any hypothesis which is formulated to explain these phenomena must take into account the following major features:

a. The lack of fuel-sodium reaction product in the regions of greatest deformation in both pins,
b. The presence of the ingot of fission products attached to the cladding of B3C,
c. The "pushed-in" appearance of the fuel in B3C (Figure 6-6),
d. The separation of the cladding flaps with attached fuel from the main portion of the fuel (Figures 6-5 and 6-6).

Further experimentation under closely controlled conditions is required to fill the large gaps in the understanding of failed fuel behavior.

7.4 FISSION GAS RELEASE

B3B

The overall release rate of fission gas in B3B was calculated to be ~ 64%. This was computed by using the maximum gas pressure (which occurred just before failure), the known void volume in the pin, and an estimated average gas temperature in the pin. (Appendix C)

B3C

Based on the measured volume of fission gas collected from B3C, the weighted average release fraction of fission gas from the fuel was 63%. (Appendix C)

Since B3C operated for an estimated 85 to 90% of its irradiation lifetime as a failed pin at 18 kW/ft, it is significant that the fission gas release rate agrees closely with data reported for unfailed mixed oxide specimens irradiated in EBR-II at comparable heat ratings and burnups.[10]

7.5 COOLANT SYSTEM CONTAMINATION

A small amount of fuel, estimated at less than 1%, did escape from the B3B fuel pin. However, the coolant system was relatively free of cesium activity. This reflects the fact that coolant circulation in B3B was stopped soon after fuel pin rupture.

B3C, in contrast to B3B, suffered significant contamination of the coolant system as shown in Tables 6-2 and 6-3. From the neutron radiograph of B3C, the loss of fuel from the pin was estimated to have been 5 to 10%. The Cs-137 release was estimated to have been slightly higher (15%). However, the cesium which plated out on the stainless steel surfaces in B3C constituted less than 1% of the cesium released from the pin. This is consistent with the observation by the Russians in the BR-5 reactor that cesium did not plate out in the primary coolant system.[11]

Analysis of coolant and leach samples in B3C showed low concentration of fission product species that are relatively insoluble in NaK. The leach samples contained the bulk of the Ru, Ze, Sb, and Ce released from the fuel pin, indicating plate out of those species in essential agreement with the BR-5 reactor data.

The data of B3C Sample CLB in Table 6-3 were converted to MeV/in.^{2} sec.* for Cs-137, Ce-144, Ru-103, Sb-125, and Zr-95 and are shown in Table 7-2. It can be seen that Ru-103 is the dominant source of activity deposited on a surface which was in a relatively cool (200°F) portion of the coolant system. Thus, cold trapping may be an effective means of removing ruthenium from sodium system.

The plutonium and uranium concentrations measured in the B3C NaK and shown in Table 6-2 indicate an upper limit of solubility at room temperature.

Table 7-2
PLATEOUT ACTIVITY ON SAMPLE CLB FROM B3C

Isotope	MeV/in.^{2} sec
Cs - 137	$(5.85)(10^5)$
Ce - 144	$(4.42)(10^5)$
Ru - 103	$(9.81)(10^8)$
Ru - 106	$(1.28)(10^6)$
Sb - 125	$(5.15)(10^5)$
Zr - 95	$(3.21)(10^7)$

REFERENCES

1. Knight, F. W., et al., *Design, Development, and Operation of A NaK-Filled Natural Convection Circulating Capsule*, Paper Presented at the International Symposium on Developments in Irradiation Capsule Technology, Pleasanton, California May 3-5, 1966.
2. McNelly, M. J., et al., *Liquid Metal Fast Breeder Reactor Design Study, 1000 MWe PuO_2 - UO_2 Fueled Plant.* Volumes I and II, January 1964, (GEAP-4418)
3. Hines, D. P., et al., *Controlled Flux Irradiations for Measurements on High Performance Fuels*, ANS Transactions, Volume 6, No. 2, November, 1963.
4. Lauritzen, T. A., *Compatibility of Urania-Plutonia with Stainless Steel and Sodium*, June, 1968, (GEAP-5633).
5. Zebroski, E. L., et al., *Irradiation Behavior of Hyper- and Hypo-Stoichiometric Plutonia- Urania Fuel At 70,000 MWd/T*, March, 1965, (GEAP-4897), p. 7-2.
6. *Sodium-Cooled Reactors Fast Ceramic Reactor Dev. Prog. Twenty-Fifth Quarterly Report, November, 1967 - January, 1968*, March, 1968, (GEAP-5584) p. 40.
7. *Sodium-Cooled Reactors Fast Ceramic Reactor Dev. Prog. - Twenty-Ninth Quarterly Report, November, 1968 - January, 1969*, February, 1969, (GEAP-5763) p. 55.
8. *Sodium-Cooled Reactors Fast Ceramic Dev. Prog. - Twenty-Sixth Quarterly Report, February - April, 1968*, June, 1968, (GEAP-5631) p. 26.
9. Perry, K. J. and Craig, C. N., *Austenitic Stainless Steel Compatibility with Mixed-Oxide Fuel*, paper presented at ANS, Winter Meeting, November 30, and December 4, 1969 in San Francisco, California.
10. *Sodium-Cooled Reactors Fast Ceramic Reactors Dev. Prog. - Twenty-Fourth Quarterly Report, August - October, 1967*, December, 1967, (GEAP-5541), p. 60.
11. Leipunskii, A. I., et al., *Experience Gained from the Operation of the BR-5 Reactor*, Paper presented at the London Conference on Fast Breeder Reactors, May 17-19, 1966.

* A more meaningful unit than atoms/in.^{2} for determining relative maintenance hazards because it factors in the half-lives and energies of the contaminant species.

APPENDIX A

FUEL PIN DESIGN DETAILS

The two fuel specimens differed from each other only in length, Specification sheets for the loaded fuel rods are shown in Tables A-1 and A-2. Figure A-1 schematically illustrates the chief design features.

Table A-1
DESIGN FEATURES OF
B3B FUEL SPECIMEN

1.	Specimen Number	B-3B
2.	Cladding Material	347 SS
3.	Inside Diameter of Cladding (in.)	0.2200
4.	Ratio U-235/U-235 + U-238 in M.O. (%)	40.0% Nom.
5.	Ratio Pu/Pu + U in M.O. (%)	25.0% Nom.
6.	Maximum Diameter Range of Pellets (in.)	
	Uranium Oxide	0.2149 - 0.2172
	Mixed Oxide	0.2162 - 0.2178
7.	Average Diameter of Pellets (in.)	
	Uranium Oxide	0.2168
	Mixed Oxide	0.2172
8.	Diametrical Gap - Fuel (in.)	
	Range	0.0022 - 0.0038
	Average	0.0028
9.	Fuel Density (% of T.D.)	
	Range	88.5% - 91.5%
	Average	90.0%
10.	Uranium Length (in.)	
	Top Blanket	8.984
	Bottom Insulator	0.500
11.	Fuel Length (in.)	22.9
12.	O/M Ratio	
	Fuel - Range	1.997 - 2.003
	Average	2.000

Table A-2
DESIGN FEATURES OF
B3C FUEL SPECIMEN

1.	Specimen Number	B-3C
2.	Cladding Material	347 SS
3.	Inside Diameter of Cladding (in.)	0.2200
4.	Ratio U-235/U-235 + U-238 in M.O. (%)	40.0% Nom.
5.	Ratio Pu/Pu + U in M.O. (%)	25.0% Nom.
6.	Maximum Diameter Range of Pellets (in.)	
	Uranium Oxide	0.2162 - 0.2169
	Mixed Oxide	0.2165 - 0.2180
7.	Average Diameter of Pellets (in.)	
	Uranium Oxide	0.2167
	Mixed Oxide	0.2176
8.	Diametrical Gap - Fuel (in.)	
	Range	0.0020 - 0.0035
	Average	0.0024
9.	Fuel Density (% of T.D.)	
	Range	89.1% - 91.4%
	Average	90.2%
10.	Uranium Length	
	Top Blanket	11.8438
	Bottom Insulation	0.7526
11.	Fuel Length (in.)	20.023
12.	O/M Mixed Oxide (Range and Average)	1.999 - 2.003
		2.001

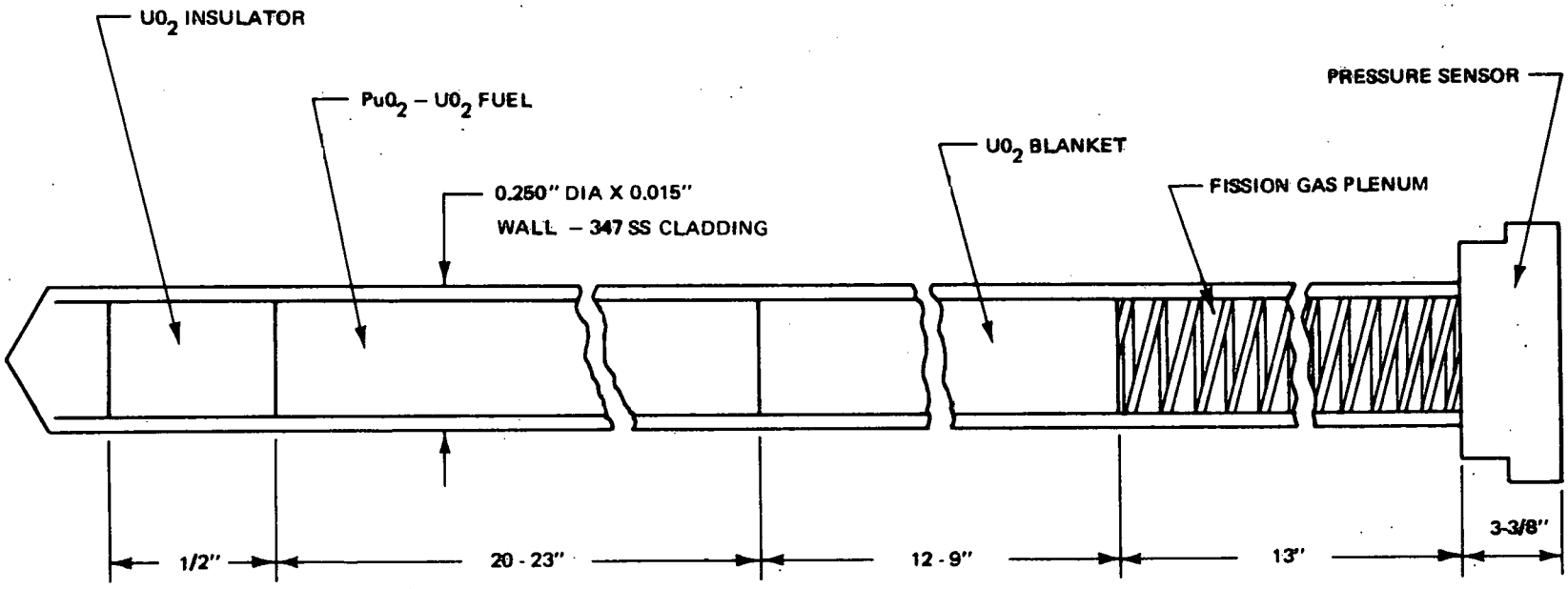

Figure A-1. Long Mixed Oxide Fuel Specimen

APPENDIX B

NATURAL CIRCULATION CAPSULE DESIGN DETAILS

The NaK-cooled natural circulation capsule has been described in detail previously. The major design features of the capsule are illustrated schematically in Figure B-1. Locations of the 23 thermocouples utilized in the capsule are also shown. The predicted NaK coolant temperatures as a function of position in the circulation loop around the chimney in B3B are shown in Figure B-2. The corresponding temperatures for B3C differed slightly from those shown for B3B due to the slightly shorter fuel pin and the higher position of the peak power region in the fuel column.

The Nak circulated up the center of the chimney past the fuel pin and down the outside of the chimney. Heat rejection from the capsule to the reactor pool water was regulated by adjustment of the composition of the binary gas (He, N_2) annulus in the outer capsule wall. Total power generation was measured by the method of water calorimetry.

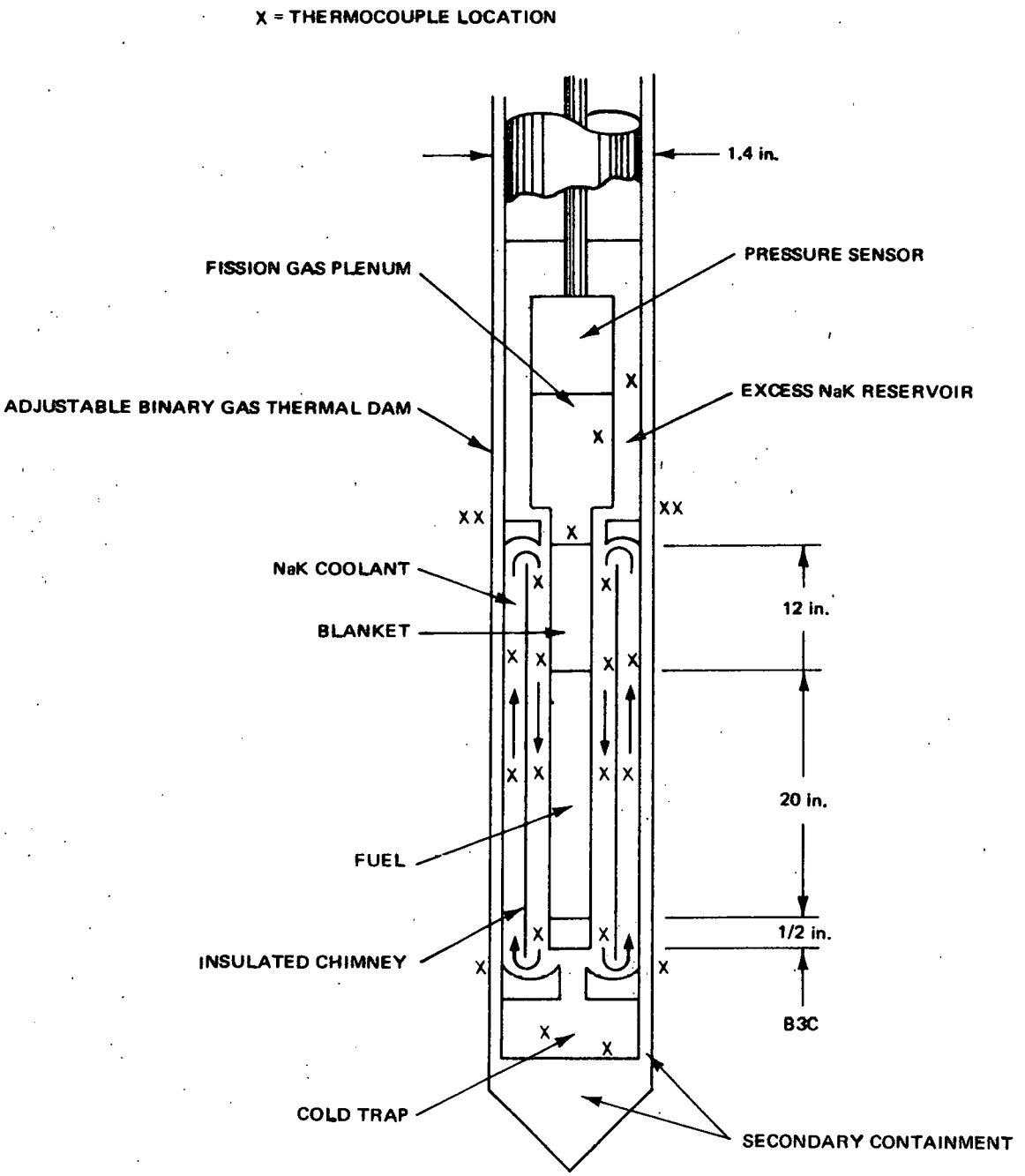

Figure B-1. Natural Circulation Capsule Design Features

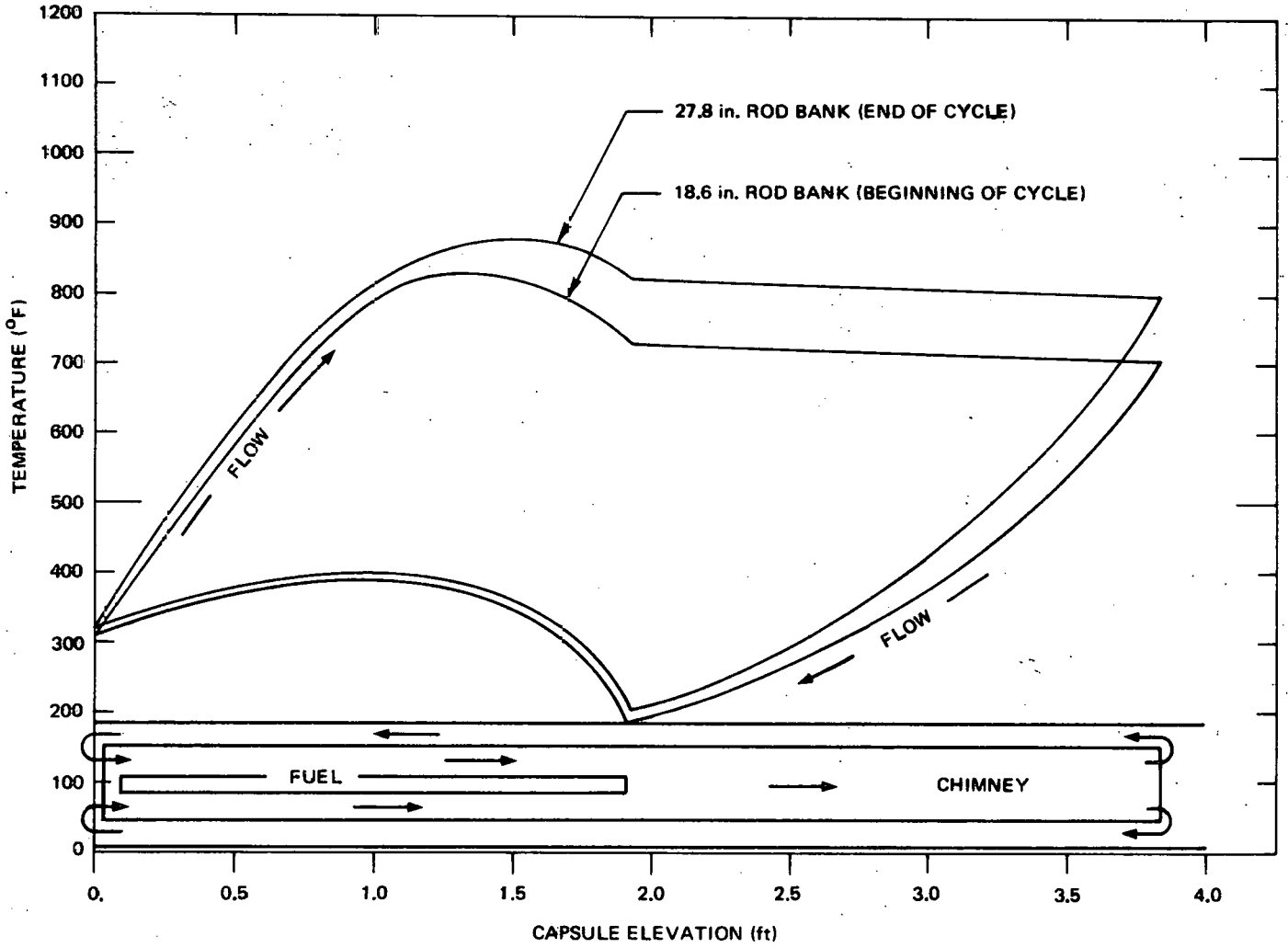

Figure B-2. Predicted Natural Convection Capsule Loop Temperatures

APPENDIX C

FISSION GAS RELEASE CALCULATIONS

In the calculations presented below, section C-1 shows the calculation of the fission gas release fraction in B3B, and C-2 gives the fission gas release fraction in B3C.

C-1 B3B Release Fraction

From Reference 2, page 6-53, the generation of stable fission gases per cc of fuel is 28.9cc (STP) after 100,000 MWd/Te burnup. The total fission gas generated in B3B was then:

$$G = \frac{28.9\text{cc gas}}{\text{cc fuel}} \ (12.6\text{cc fuel}) \ \frac{13{,}500 \text{ MWd/Te ave. burnup}}{100{,}000 \text{ MWd/Te}}$$

$$= 49\text{cc (STP)}$$

The B3B pressure sensor indicated a maximum of 76 psia @ an average gas temperature of 470°F. This is equivalent to 43.8 psia @ 77°F. Given that the total void space in the B3B pin was 16.8cc and that the pin was originally filled with helium to 14.7 psia, the amount of fission gas released from the fuel may be obtained by the following ratio:

$$\frac{16.8 + R}{16.8} = \frac{43.8 \text{ psia}}{14.7 \text{ psia}}$$

Where R, the number of cc (STP) of gas released from the B3B pin, is found to equal 31.2.

The overall release fraction in B3B is then obtained by:

$$F = \frac{\text{cc gas released}}{\text{cc gas generated}}$$

$$= \frac{31.2}{49}$$

$$= 0.64 \text{ or } 64\%$$

C-2 B3C Release Fraction

From Table 6-1, the amount of stable fission gases contained in the cover gas was 0.376 (239 cc) = 89.9 cc. Again, the generation of stable fission gases per cc of fuel is 28.9 cc (STP) after 100,000 MWd/Te burnup. The fission gas release fraction from the B3C fuel specimen is, therefore, given by

$$F = \frac{\text{cc gas released}}{\text{cc gas generated}}$$

$$= \frac{89.9\text{cc}}{28.9 \left(\frac{45{,}000}{100{,}000}\right)} \ (11.0 \text{ cc fuel})$$

$$= 0.63 \text{ or } 63\%$$

DISTRIBUTION

Director, Contracts Division
U. S. Atomic Energy Commission
San Francisco Operations Office
2111 Bancroft Way
Berkeley, California 94704 — 1

RDT Site Office
U. S. Atomic Energy Commission
General Electric Company
310 DeGuigne Drive
Sunnyvale, California 94086 — 1

Chief, California Patent Group
U. S. Atomic Energy Commission
San Francisco Operations Office
P. O. Box 808
Livermore, California 94550 — 1

Manager
Westinghouse Electric Corporation
Advanced Reactors Division
P. O. Box 158
Madison, Pennsylvania 15663 — 1

Division of Reactor Development
and Technology, Headquarters
U. S. Atomic Energy Commission
Washington, D. C. 20545
Attn: Assistant Director,
Engineering Standards — 1

Division of Reactor Development
and Technology, Headquarters
U. S. Atomic Energy Commission
Washington, D. C. 20545
Attn: Assistant Director,
Nuclear Safety — 1

Division of Reactor Development
and Technology, Headquarters
U. S. Atomic Energy Commission
Washington, D. C. 20545
Attn: Assistant Director,
Plant Engineering — 1

Division of Reactor Development
and Technology, Headquarters
U. S. Atomic Energy Commission
Washington, D. C. 20545
Attn: Assistant Director,
Program Analysis — 1

Division of Reactor Development
and Technology, Headquarters
U. S. Atomic Energy Commission
Washington, D. C. 20545
Attn: Assistant Director,
Project Management — 2

Division of Reactor Development
and Technology, Headquarters
U. S. Atomic Energy Commission
Washington, D. C. 20545
Attn: Assistant Director,
Reactor Engineering — 1

Division of Reactor Development
and Technology, Headquarters
U. S. Atomic Energy Commission
Washington, D. C. 20545
Attn: Assistant Director,
Reactor Technology — 1

Division of Reactor Development
and Technology, Headquarters
U. S. Atomic Energy Commission
Washington, D. C. 20545
Attn: Chief, Fuels and
Materials Branch — 3

Division of Reactor Development
and Technology, Headquarters
U. S. Atomic Energy Commission
Washington, D. C. 20545
Attn: Chief, Fuel Engineering
Branch — 1

Division of Reactor Development
and Technology, Headquarters
U. S. Atomic Energy Commission
Washington, D. C. 20545
Attn: Chief, Reactor Vessels
Branch — 1

Assistant Director for
Pacific Northwest Programs, RDT
U. S. Atomic Energy Commission
P. O. Box 550
Richland, Washington 99352 — 1

RDT Site Office
U. S. Atomic Energy Commission
Argonne National Laboratory
Building 2,
Argonne, Illinois 60439 — 1

RDT Site Office
U. S. Atomic Energy Commission
Atomics International
P. O. Box 1446
Canoga Park, California 91304 — 1

RDT Site Office
U. S. Atomic Energy Commission
Argonne National Laboratory
P. O. Box 2108
Idaho Falls, Idaho 83401 — 2

RDT Senior Site Representative — 1
U. S. Atomic Energy Commission
P. O. Box 2325
San Diego, California 92112

Division of Naval Reactors — 1
Chief, Nuclear Materials Branch
U. S. Atomic Energy Commission
Washington, D. C. 20545

Director — 2
Division of Reactor Licensing
U. S. Atomic Energy Commission
Washington, D. C. 20545

Director — 2
Metallurgy Division
Argonne National Laboratory
9700 South Cass Avenue
Argonne, Illinois 60439

Manager, FFTF Project — 6
Pacific Northwest Laboratory
P. O. Box 999
Richland, Washington 99352

Manager — 1
Chemistry and Metallurgy Division
Pacific Northwest Laboratory
P. O. Box 999
Richland, Washington 99352

RDT Site Office — 1
U. S. Atomic Energy Commission
Oak Ridge National Laboratory
P. O. Box X
Oak Ridge, Tennessee 37830

Director — 2
Division of Reactor Standards
U. S. Atomic Energy Commission
Washington, D. C. 20545

Division of Technical — 3*,50**
Information Extension
U. S. Atomic Energy Commission
P. O. Box 62
Oak Ridge, Tennessee 37831

Director — 2
LMFBR Program Office
Argonne National Laboratory
9700 South Cass Avenue
Argonne, Illinois 60439

Director — 1
Chemical Engineering Division
Argonne National Laboratory
9700 South Cass Avenue
Argonne, Illinois 60439

* submitted with transmittal for AEC-426.
** submitted for transmittal to recipient under UKAEA/USAEC and EURATOM/USAEC Fast Breeder Reactor Information Exchange arrangements.

FFTF Fuels Department — 2
Pacific Northwest Laboratory
P. O. Box 999
Richland, Washington 99352

Division Leader (CMB) — 1
Chemistry and Metallurgy Division
Los Alamos Scientific Laboratory
P. O. Box 1663
Los Alamos, New Mexico 87544

Director — 1
Metallurgy and Materials
Science Division
Brookhaven National Laboratory
Upton, New York 11973

Division Chief, M & S Division — 1
NASA - Lewis Research Center
21000 Brookpark Road
Cleveland, Ohio 44135

Division Leader, Inorganic Materials — 1
Chemistry Department Lawrence Radiation
Lawrence Radiation Laboratory
P. O. Box 808
Livermore, California 94550

General Manager — 1
Westinghouse Electric Corporation
Bettis Atomic Power Laboratory
P. O. Box 79
West Mifflin, Pennsylvania 15122

Associate Manager — 1
Materials Engineering Department
Battelle Memorial Institute
Columbus Laboratories
505 King Avenue
Columbus, Ohio 43201

Manager, Nuclear Laboratories — 1
Combustion Engineering Inc.
Nuclear Division
Prospect Hill Road
Windsor, Connecticut 06095

Manager, Plutonium Chemistry — 1
and Ceramics Fuels Development
Nuclear Materials and Equipment
Corporation
Plutonium Laboratory
Leechburg, Pennsylvania 15656

Head, Fuels and Materials — 1
Atomic Power Development Associates
1911 First Street
Detroit, Michigan 48226

Director — 2
Metals and Ceramics Division
Oak Ridge National Laboratory
P. O. Box X
Oak Ridge, Tennessee 37830

Director, Liquid Metal
Engineering Center
Atomics International
P. O. Box 1449
Canoga Park, California 91304 — 1

Manager—Advanced Development Activity
General Electric Company
Knolls Atomic Power Laboratory
P. O. Box 1072
Schenectady, New York 12301 — 1

Director, LMFBR Technology Program
Atomics International
P. O. Box 309
Canoga Park, California 91304 — 1

Director
Nuclear Development Center
The Babcock and Wilcox Company
Atomic Energy Division
Lynchburg, Virginia 24501 — 1

Laboratory Assistant Director
Gulf General Atomic Incorporated
P. O. Box 608
San Diego, California 92112 — 1

Manager, Research
United Nuclear Corporation
Research and Engineering Center
Grasslands Road
Elmsford, New York 10523 — 1

Director
Nuclear Safety Program
Oak Ridge National Laboratory
P. O. Box Y
Oak Ridge, Tennessee 37830 — 3

K-2 Group Leader
Reactor Division
Los Alamos Scientific Laboratory
P. O. Box 1663
Los Alamos, New Mexico 87544 — 1

Westinghouse Electric Corporation
Technical Director
Advanced Reactors Division
P. O. Box 158
Madison, Pennsylvania 15663 — 2

Manager
Liquid Metal Information Center
Atomics International
P. O. Box 1449
Canoga Park, California 91304 — 1

Irradiation Coordinator
EBR-II Project
Argonne National Laboratory
P. O. Box 2528
Idaho Falls, Idaho 83401 — 1

Experiment Manager
EBR-II Project
Argonne National Laboratory
9700 South Cass Avenue
Argonne, Illinois 60439 — 1

Director
Reactor Analysis and Safety Division
Argonne National Laboratory
9700 South Cass Avenue
Argonne, Illinois, 60439 — 5